



Design, synthesis of novel 4,5-dihydroisoxazole-containing benzamide derivatives as highly potent FtsZ inhibitors capable of killing a variety of MDR *Staphylococcus aureus*

Di Song, Fangchao Bi, Nan Zhang, Yinhui Qin, Xingbang Liu, Yuetai Teng, Shutao Ma*

Department of Medicinal Chemistry, Key Laboratory of Chemical Biology (Ministry of Education), School of Pharmaceutical Sciences, Cheeloo College of Medicine, Shandong University, 44 West Wenhua Road, Jinan 250012, China

ARTICLE INFO

Keywords:

4,5-Dihydroisoxazole-containing benzamide
Design and synthesis
Antibacterial activity
FtsZ inhibitor
Structure-activity relationships

ABSTRACT

Antibiotic resistance among clinically significant bacterial pathogens, such as methicillin-resistant *Staphylococcus aureus* (MRSA) and vancomycin-resistant *S. aureus* (VRSA) is becoming a prevalent threat to public health, and new antibacterial agents with novel mechanisms of action hence are in an urgent need. As a part of continuing effort to develop antibacterial agents, we rationally designed and synthesized two series of 4,5-dihydroisoxazol-5-yl and 4,5-dihydroisoxazol-3-yl-containing benzamide derivatives that targeted the bacterial cell division protein FtsZ. Evaluation of their activity against a panel of Gram-positive and -negative pathogens revealed that compound **A16** possessing the 4,5-dihydroisoxazol-5-yl group showed outstanding antibacterial activity (MIC, ≤ 0.125 – $0.5 \mu\text{g/mL}$) against various testing strains, including methicillin-resistant, penicillin-resistant and clinical isolated *S. aureus* strains. Besides, further mouse infection model revealed that **A16** could be effective *in vivo* and non-toxic to Hela cells. Finally, a detailed discussion of structure-activity relationships was conducted, referring to the docking results. It is worth noting that substituting a 4,5-dihydroisoxazole ring for the isoxazole ring not only broadened the antibacterial spectrum but also resulted in a significant increase in antibacterial activity against *S. aureus* strains. Taken together, these results suggest a promising chemotype for the development of new FtsZ-targeting bactericidal agents.

1. Introduction

There is a serious threat to public health due to the increasing of antimicrobial resistance (AMR),¹ and the innovation rate of new antibiotics cannot keep up with the emergence of antibiotic-resistant bacteria, which definitely aggravates this problem.² Therefore, to address the increasing serious antibiotic resistance, new classes of molecules with novel action mode or newer generations of previously used antibiotics should be urgently developed.³

Filamentous temperature-sensitive mutant Z (FtsZ) is a key protein for bacterial cell division and an attractive target for new antibiotics development.⁴ A number of FtsZ-interacting compounds have been discovered, some of which possess potent antibacterial activity, just listing several of them being just listed for example in Fig. 1.^{5–9} Among these FtsZ-targeting compounds, benzamide derivatives family is an attractive point and has been extensively investigated by different research groups. This continuous research finally culminated in the development of PC190723 which was derived from the weak inhibitor 3-

methoxybenzamide (3-MBA).^{10,11} Further investigations would be focused on the optimizing its drug-like properties.^{12–15}

Most benzamide derivatives that have been studied contain parallel-connected or series-connected heteroaromatic rings which are planar rigid structures at the 3-O-position, such as PC190723 and compound **1** (Fig. 1). Considering the amino acid residues on the inner surface of the binding pocket of FtsZ are less likely to shape flat regions, we surmise that noncoplanar heterocyclic structure could form more suitable interaction with the protein FtsZ though there is an induced fit binding mode between molecule and target site. According to the above hypothesis and a continuation of effort to further develop benzamide derivatives as antibacterial agents, we tried to introduce a noncoplanar heterocyclic structure to increase the flexibility and conformational diversity of the target molecules, in order to form more changeable molecular skeleton. We previously reported on some potent antibacterial compounds by introducing an isoxazole ring to connect the benzamide and the aromatic moieties.¹⁶ In this paper, we further designed a series of 4,5-dihydroisoxazol-5-yl-containing benzamide

* Corresponding author.

E-mail address: mashutao@sdu.edu.cn (S. Ma).

<https://doi.org/10.1016/j.bmc.2020.115729>

Received 3 June 2020; Received in revised form 30 July 2020; Accepted 19 August 2020

Available online 27 August 2020

0968-0896/ © 2020 Elsevier Ltd. All rights reserved.

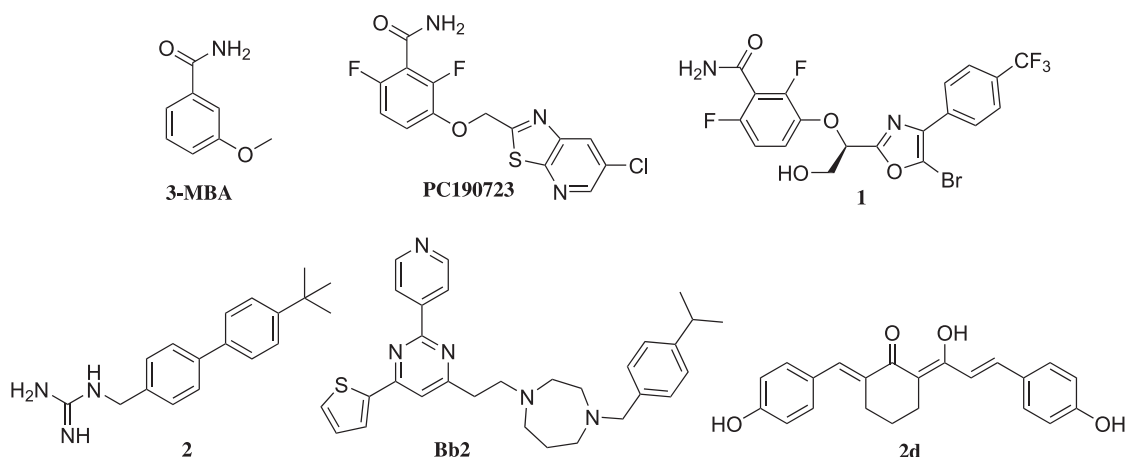


Fig. 1. Chemical structures of some FtsZ inhibitors.

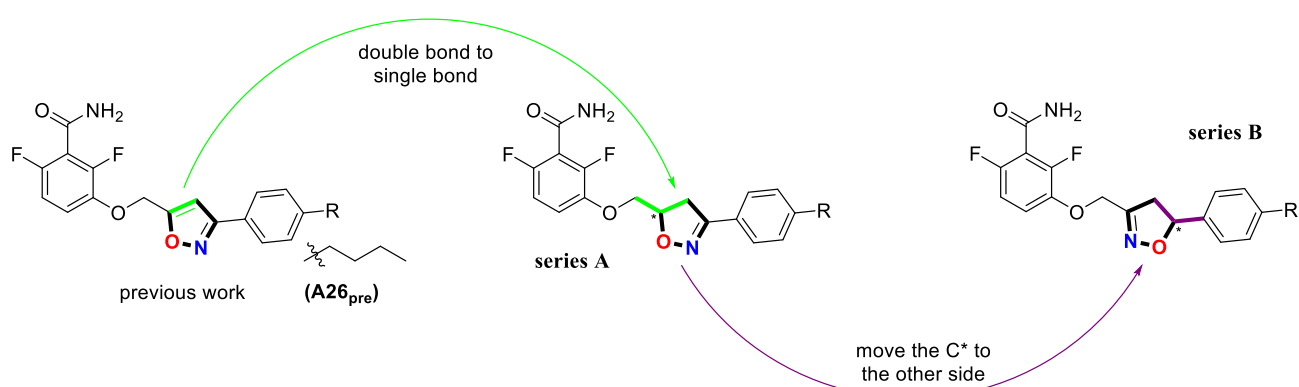


Fig. 2. Brief design process of the 4,5-dihydroisoxazole benzamide derivatives.

derivatives (series A) by substituting a nonplanar 4,5-dihydroisoxazole ring for the isoxazole ring in the structure. This structural change alters the planarity of five-membered isoxazole heterocycle and can cause a noncoplanar skeleton and more diverse conformation when the C–O or C–C bond in the structure twirls. On this basis, we designed another series of 4,5-dihydroisoxazol-3-yl-containing benzamide derivatives (series B) by altering the connection of the 4,5-dihydroisoxazole ring in the structure. The above brief design strategy is illustrated in Fig. 2. Here we reported the synthesis and *in vitro* antibacterial activity of the series A and B. The cell morphology and the FtsZ polymerization as on-target effect were also performed. The outstanding compounds were selected to further evaluate their plasma stability, *in vivo* antimicrobial activity and cytotoxicity, and ultimately, compound A16 was identified to be a novel and potent lead antibacterial agent as an FtsZ inhibitor.

2. Chemistry

2.1. Synthesis of 4,5-dihydroisoxazol-5-yl-containing benzamide derivatives (series A)

The synthetic route for the series A is shown in Scheme 1. Commercially available 2,4-difluorophenol **3** was protected by benzyl group, and then treated with dry ice in the presence of *n*-BuLi, giving benzoic acid **4**. The acid **4** was converted to benzamide **5** using oxalyl chloride, followed by ammonium carbonate. After deprotection of the benzyl group, alkylation of **6** with 3-bromopropylene afforded key intermediate **7**. Finally, cyclization of **7** with various oximes **9** that were prepared from commercially available or synthesized aldehyde **8** in the presence of chloramine-T gave the 4,5-dihydroisoxazol-5-yl-containing benzamide derivatives **A1**–**A27**.

2.2. Synthesis of 4,5-dihydroisoxazol-3-yl-containing benzamide derivatives (series B)

The synthetic route for series B is listed in Scheme 2. Commercially available or synthesized benzaldehydes **8** were converted to corresponding styrenes **10** which were then cyclized with ethyl nitroacetate to afford the intermediates **11**.¹⁷ Reduction with NaBH₄ and then bromination provided the intermediates **12**, which were then condensed with **6** to afford the 4,5-dihydroisoxazol-3-yl-containing benzamide derivatives **B1**–**B18**.

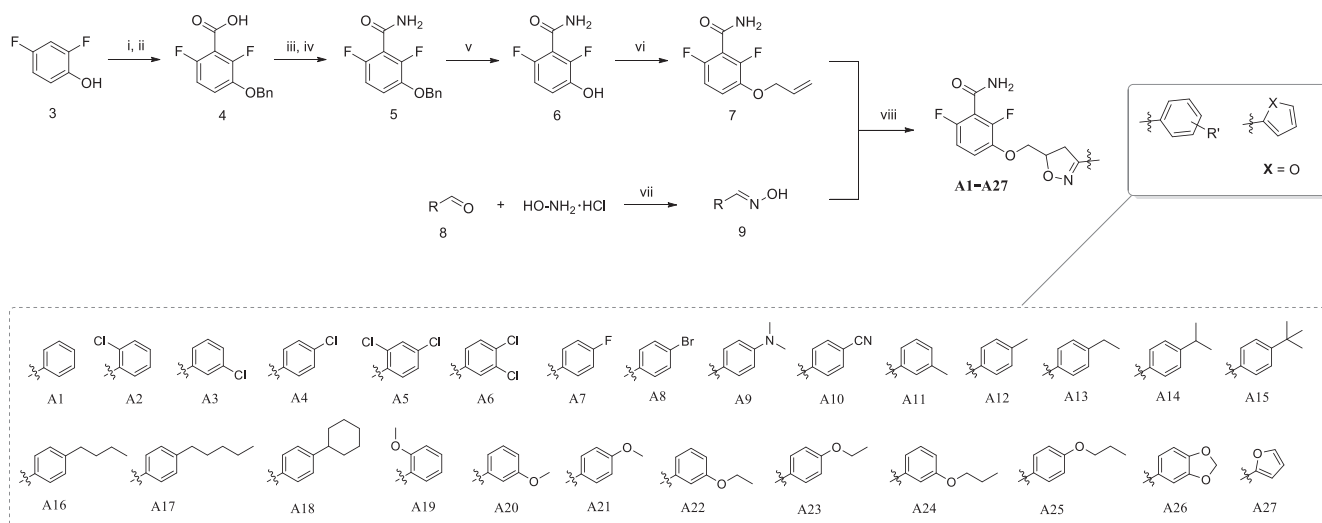
2.3. Analysis and determination of the absolute configuration of representative compound A16

Representative compound **A16** that incorporates a chiral carbon atom, has two isomers of R- and S-configurations. The high-performance liquid chromatography (HPLC) diagram demonstrated that the two enantiomers of **A16** had the same peak area, and we successfully resolved the two enantiomers by preparative HPLC. Then, the absolute configurations of the two enantiomers were further confirmed by the agreement exhibiting in experimental and calculated electronic circular dichroism (ECD) spectra (Fig. 3) (Supplementary data, Figs. S1–S3).

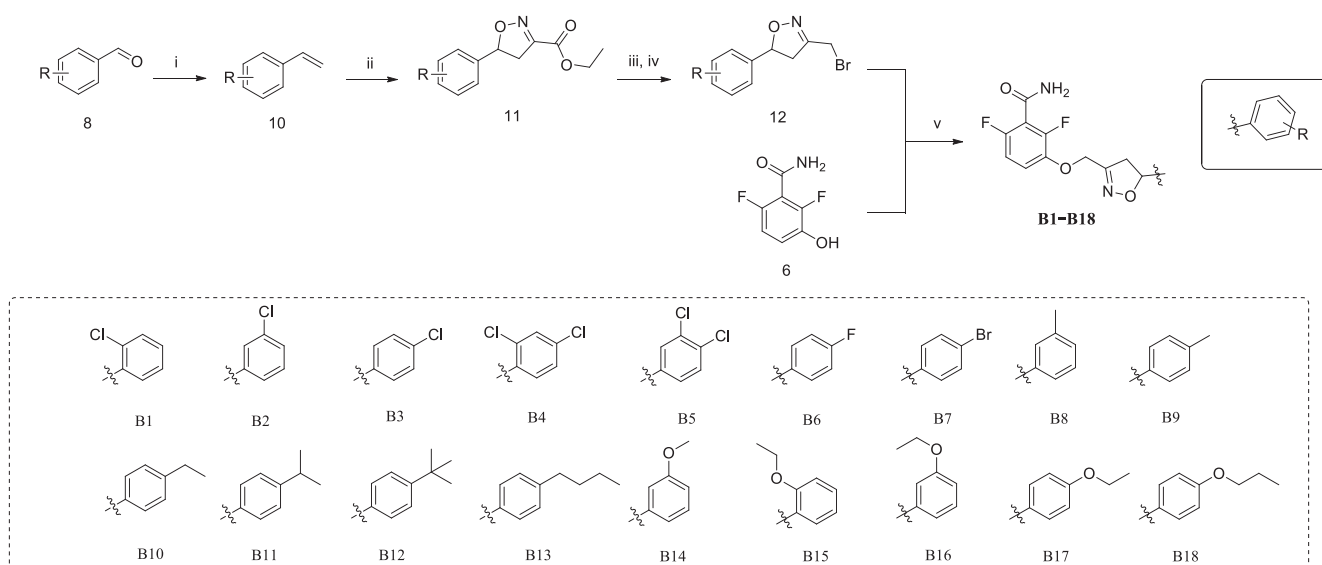
3. Results and discussion

3.1. *In vitro* antibacterial activity of series A and B

The synthesized compounds shown in Scheme 1 and 2 were tested for their *in vitro* antibacterial activity through broth microdilution procedures described in the Clinical and Laboratory Standards Institute



Scheme 1. Synthetic route for series A. Reagents and conditions: (i) benzyl chloride, K_2CO_3 , NaI, MeCN, 45 °C; (ii) *n*-BuLi, dry ice, THF, 50 °C to rt; (iii) oxalyl chloride, DMF, DCM, rt; (iv) ammonium carbonate, DCM, rt; (v) 10% Pd/C, ammonium formate, EtOH, 65 °C; (vi) 3-bromopropyne, K_2CO_3 , DMF, 35 °C; (vii) NaOH, $H_2O/EtOH$, rt; (viii) chloramine-T, EtOH, rt.



Scheme 2. Synthetic route for series B. Reagents and conditions: (i) methyltriphenylphosphonium bromide, NaH, THF, N_2 protection; 0 °C to rt; (ii) ethyl ni-troacetate, triethylenediamine, EtOH, 78 °C; (iii) $NaBH_4$, THF/MeOH, rt; (iv) Ph_3P , CBr_4 , DCM, rt; (v) K_2CO_3 , DMF, 35 °C.

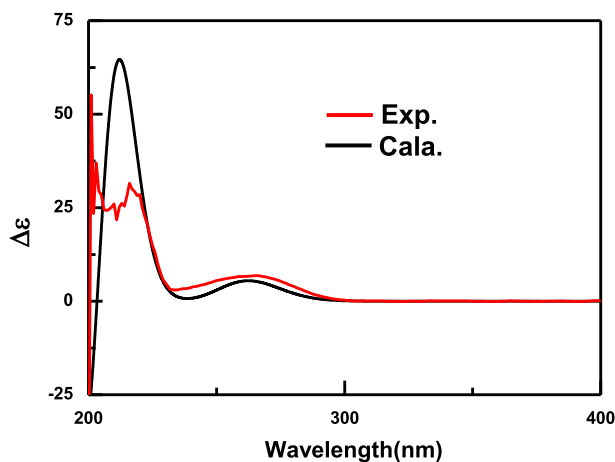


Fig. 3. Experimental ECD (red) and calculated ECD (black) of A16-S.

Table 1
The *in vitro* antibacterial activity of the 4,5-dihydroisoxazol-5-yl-containing benzamide derivatives (series A).

Comp	Minimum inhibitory concentration/MIC ($\mu\text{g/mL}$)							
	<i>B. subtilis</i> ATCC9372	<i>B. pumilus</i> CMCC63202	<i>S. aureus</i> ATCC25923	<i>S. aureus</i> ATCC43300 ^a	<i>S. aureus</i> PR ^b	<i>S. aureus</i> CI ^c	<i>E. coli</i> ATCC25922	<i>P. aeruginosa</i> ATCC27853
A1	16	64	> 64	> 64	> 64	NT	> 64	> 64
A2	16	64	> 64	> 64	> 64	NT	> 64	> 64
A3	2	8	16	32	32	NT	> 64	> 64
A4	8	8	32	32	32	NT	> 64	> 64
A5	4	2	16	32	32	NT	> 64	> 64
A6	2	> 64	> 64	> 64	> 64	NT	> 64	> 64
A7	8	32	64	64	64	NT	> 64	> 64
A8	2	4	32	32	32	NT	> 64	> 64
A9	16	64	> 64	> 64	> 64	NT	> 64	> 64
A10	32	> 64	> 64	> 64	> 64	NT	> 64	> 64
A11	16	8	32	16	64	NT	> 64	> 64
A12	16	16	32	32	> 64	NT	> 64	> 64
A13	0.5	2	8	8	16	NT	> 64	> 64
A14	≤ 0.125	≤ 0.125	4	4	16	NT	> 64	> 64
A15	0.25	≤ 0.125	4	2	4	4	> 64	> 64
A16	0.5	≤ 0.125	0.5	0.25	0.5	0.5	> 64	> 64
A17	0.5	≤ 0.125	> 64	> 64	> 64	NT	> 64	> 64
A18	> 64	> 64	> 64	> 64	> 64	NT	> 64	> 64
A19	> 64	> 64	> 64	> 64	> 64	NT	> 64	> 64
A20	8	32	> 64	> 64	> 64	NT	> 64	> 64
A21	8	32	> 64	> 64	> 64	NT	> 64	> 64
A22	4	8	32	32	32	NT	> 64	> 64
A23	4	16	64	64	> 64	NT	> 64	> 64
A24	4	2	16	16	32	NT	> 64	> 64
A25	4	4	> 64	> 64	> 64	NT	> 64	> 64
A26	16	16	64	64	64	NT	> 64	> 64
A27	64	> 64	> 64	> 64	> 64	NT	> 64	> 64
A16-R	0.25	0.5	4	2	1	2	> 64	> 64
A16-S	≤ 0.125	≤ 0.125	0.25	≤ 0.125	0.25	≤ 0.125	> 64	> 64
PC	0.5	0.5	1	1	1	1	> 64	> 64
CIP ^d	2	8	8	16	> 64	16	8	4
LIN ^e	0.5	1	2	2	1	1	> 64	> 64
Ery ^f	≤ 0.125	≤ 0.125	≤ 0.125	> 64	> 64	> 64	16	32

^a *S. aureus* ATCC43300: methicillin-resistant strain.

^b *S. aureus* PR: penicillin-resistant strain.

^c *S. aureus* CI: clinical isolated strain, not characterized.

^d CIP: ciprofloxacin.

^e LIN: linezolid.

^f ERY: erythromycin.

(CLSI) guidelines.¹⁸ MIC (minimal inhibitory concentration) values for all the compounds were determined on a panel of sensitive and resistant bacterial strains. PC (PC190723), CIP (ciprofloxacin), LIN (linezolid) and ERY (erythromycin) were included as references. The MIC results shown in Table 1 and Table 2 indicates that some of the 4,5-dihydroisoxazole-containing benzamide derivatives display superior or equivalent efficacy to the clinical antibiotics and PC evaluated in this study.

In the series A, **A14** demonstrated the best activity against *B. subtilis* ATCC9372 with a MIC value ≤ 0.125 $\mu\text{g/mL}$, comparable to that of CIP and ERY. Besides, **A13**, **A15**, **A16** and **A17** also showed excellent activity against *B. subtilis* ATCC9372, better than or equal to PC and LIN. **A14**, **A15**, **A16** and **A17** demonstrated potent activity against *B. pumilus* CMCC63202 with the MIC values ≤ 0.125 $\mu\text{g/mL}$, better than PC (0.5 $\mu\text{g/mL}$), CIP (8 $\mu\text{g/mL}$) and LIN (1 $\mu\text{g/mL}$). In particular, **A16** not only displayed the best antibacterial activity against *S. aureus* ATCC25923 with a low MIC value of 0.5 $\mu\text{g/mL}$ but also effectively inhibited the growth of three resistant *S. aureus* strains. For example, the antibacterial activity of **A16** against *S. aureus* ATCC43300 was 4-, 64- and 8-fold more active than that of the positive controls PC (1 $\mu\text{g/mL}$), CIP (16 $\mu\text{g/mL}$) and LIN (2 $\mu\text{g/mL}$). Moreover, **A16** showed remarkable activity against *S. aureus* PR with a MIC value of 0.5 $\mu\text{g/mL}$, which was 2- and 2-fold more potent than that of PC and LIN. Notably, although the clinical isolated *S. aureus* (CI) pathogen had a definite resistance to CIP and ERY, it could not escape suppression at 0.5 $\mu\text{g/mL}$

of **A16**. There is no doubt that **A16** is the best compound in the series A due to its outstanding activity against all the tested Gram-positive bacteria strains.

Although **A16-R** and **A16-S** are a pair of enantiomers, **A16-S** displayed not only more potent antibacterial activity than **A16-R**, but also increased activity compared with **A16**. In particular, **A16-S** exhibited the best antibacterial activity against all the tested Gram-positive pathogens with the MIC values ranging from ≤ 0.125 to 0.25 $\mu\text{g/mL}$, better than or equal to PC, CIP, LIN or ERY. For example, **A16-S** exhibited excellent activity against *B. subtilis* ATCC9372 and *B. pumilus* CMCC63202 with the MIC values of ≤ 0.125 $\mu\text{g/mL}$, which were equal to that of ERY. Moreover, the antibacterial activity of **A16-S** against three resistant *S. aureus* strains were stronger than that of the positive controls. However, **A16-S** could not inhibit the growth of Gram-negative pathogens. The above results indicate that **A16-S** plays a significant role in the antibacterial activity of **A16**, which is worthy of further study.

In the series B, **B13** derived from exchanging the N and O atom's relative position in the 4,5-dihydroisoxazole ring was found to display excellent activity against *B. subtilis* ATCC9372 with a MIC value of ≤ 0.125 $\mu\text{g/mL}$, comparable to ERY. **B3**, **B4**, **B10**, **B11** and **B12** showed moderate antibacterial activity against *B. subtilis* ATCC9372 with the MIC values of 2–4 $\mu\text{g/mL}$. Notably, **B4** and **B13** exerted stronger activity against *B. pumilus* CMCC63202 than the others with the MIC values 0.5 $\mu\text{g/mL}$, better than or equal to that of LIN (1 $\mu\text{g/mL}$)

Table 2
The *in vitro* antibacterial activity of the 4,5-dihydroisoxazol-3-yl-containing benzamide derivatives (series B).

Comp	Minimum inhibitory concentration/MIC ($\mu\text{g/mL}$)							
	<i>B. subtilis</i> ATCC9372	<i>B. pumilus</i> CMCC63202	<i>S. aureus</i> ATCC25923	<i>S. aureus</i> ATCC43300 ^a	<i>S. aureus</i> PR ^b	<i>S. aureus</i> CI ^c	<i>E. coli</i> ATCC25922	<i>P. aeruginosa</i> ATCC27853
B1	16	32	> 64	> 64	> 64	NT	> 64	> 64
B2	64	> 64	> 64	> 64	> 64	NT	> 64	> 64
B3	4	16	64	32	64	NT	> 64	> 64
B4	2	0.5	32	16	32	16	> 64	> 64
B5	16	> 64	> 64	> 64	> 64	NT	> 64	> 64
B6	16	64	> 64	> 64	> 64	NT	> 64	> 64
B7	8	32	> 64	32	> 64	NT	> 64	> 64
B8	64	> 64	> 64	> 64	> 64	NT	> 64	> 64
B9	16	64	> 64	> 64	> 64	NT	> 64	> 64
B10	4	16	64	64	> 64	NT	> 64	> 64
B11	4	8	64	64	> 64	NT	> 64	> 64
B12	2	4	64	32	32	NT	> 64	> 64
B13	≤ 0.125	0.5	8	4	4	NT	> 64	> 64
B14	> 64	> 64	> 64	> 64	> 64	NT	> 64	> 64
B15	> 64	> 64	> 64	> 64	> 64	NT	> 64	> 64
B16	64	> 64	> 64	> 64	> 64	NT	> 64	> 64
B17	16	64	> 64	64	> 64	NT	> 64	> 64
B18	8	32	> 64	64	> 64	NT	> 64	> 64
PC	0.5	0.5	1	1	1	1	> 64	> 64
CIP ^d	2	8	8	16	> 64	16	8	4
LIN ^e	0.5	1	2	2	1	1	> 64	> 64
Ery ^f	≤ 0.125	≤ 0.125	≤ 0.125	> 64	> 64	> 64	16	32

^a *S. aureus* ATCC43300: methicillin-resistant strain.

^b *S. aureus* PR: penicillin-resistant strain.

^c *S. aureus* CI: clinical isolated strain, not characterized.

^d CIP: ciprofloxacin;

^e LIN: linezolid;

^f ERY: erythromycin.

Table 3
Comparison of MIC and MBC Values for **A16** in four strains of *S. aureus*.

Comp	MBC ($\mu\text{g/mL}$)	MIC ($\mu\text{g/mL}$)	MBC/MIC
Susceptible <i>S. aureus</i> (ATCC25923)			
A16	0.5	0.5	1
LIN	> 64	2	> 32
CLA	4	0.125	32
Methicillin-resistant <i>S. aureus</i> (ATCC43300)			
A16	0.5	0.25	2
LIN	> 64	2	> 32
CLA	N/A	> 64	N/A
Penicillin-resistant <i>S. aureus</i>			
A16	1	0.5	2
LIN	> 64	1	> 64
CLA	N/A	> 64	N/A
Clinical isolated <i>S. aureus</i>			
A16	0.5	0.5	1
LIN	64	1	64
CLA	N/A	> 64	N/A

^aLIN and CLA are included as control agents.

^bN/A, not applicable.

and PC (0.5 $\mu\text{g/mL}$). Besides, **B13** demonstrated moderate antibacterial activity against three *S. aureus* strains with the MIC values of 4–8 $\mu\text{g/mL}$, which is slightly lower than that of PC and LIN.

3.2. Bactericidal or bacteriostatic assay

The primary *in vitro* antibacterial activity of **A16** highlighted by the results in Table 1 prompted us to further investigate whether its activity was bactericidal or bacteriostatic. Therefore, the MBC (minimal bactericidal concentration) values of **A16** against susceptible (ATCC25923), methicillin-resistant (ATCC43300), penicillin-resistant and clinical isolated *S. aureus* strains were tested and compared with its

corresponding MIC values. Clinical drug LIN and clarithromycin (CLA) were used as controls in the *S. aureus* determinations. The results shown in Table 3 indicate that the MBC/MIC ratios of LIN and CLA are ≥ 32 , which was observed as bacteriostatic activity. Significantly, **A16** exhibited almost equivalent MBC and MIC values (i.e., MBC/MIC ratio of 1 and 2) for both susceptible and resistant *S. aureus*, which indicates its bactericidal mode clearly.

3.3. Kinetics of the bactericidal activity

In view of its bactericidal nature, we next investigated the time-kill curves of **A16** on a clinical isolated *S. aureus* strain. As shown in Fig. 4, the growth trend of the bacterial strain was suppressed obviously when incubated with $0.5 \times \text{MIC}$ of **A16** compared with no drug treated curve. At the concentration of $1 \times \text{MIC}$, $2 \times \text{MIC}$ and $4 \times \text{MIC}$, **A16** could reduce the viable counts below the lowest detectable limit (10^3 CFU/mL) after incubation for 24, 12 and 9 h, respectively. The time-kill curves of different concentration gradient indicate that the speed at which **A16** killed *S. aureus* is positively correlated with its concentration. The higher concentration resulted in the faster rate of killing.

3.4. Effects on the morphology of *B. subtilis* cells and *S. aureus* cells

We have known that FtsZ-targeting compounds such as PC190723 can inhibit bacterial cell division and result in bacterial cell elongation or enlargement.¹⁹ Thus we next explored the effect of **A16** on the bacterial cell morphology through microscopic observation to confirm whether its mode of action was associated with alteration of FtsZ. As shown in Fig. 5, compared with untreated bacterial cells, **A16** elongates the cell length of *B. subtilis* and enlarges the cell size of *S. aureus* ATCC CI significantly at $0.5 \times \text{MIC}$ concentration, which is consistent with other reported 3-substituted benzamide derivatives.^{11,20} Fig. 5 (A) indicates that the normal cells of *B. subtilis* have characteristic short rod morphology with the average length of 2.28 μm ($n = 15$, Standard

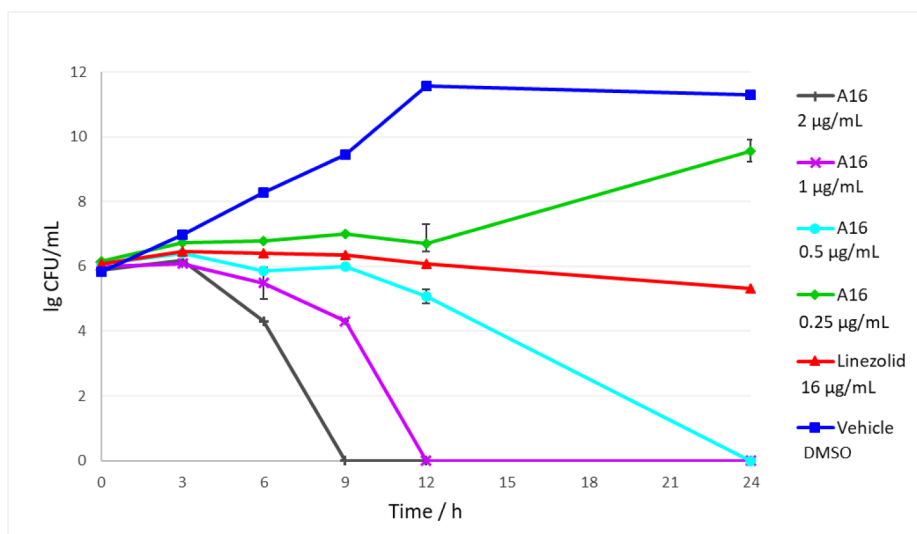


Fig. 4. Time-kill curves for clinical isolated *S. aureus* at different concentrations of A16.

Deviation = 0.29). After treatment with A16 (0.25 µg/mL), almost all the bacteria showed iconic elongated phenotype in rod-shaped *B. subtilis* cells with the average length of 29.33 µm ($n = 15$, $SD = 4.56$) (Fig. 5 (B) and 5 (C)). Fig. 5 (D) points out that the normal cell of *S. aureus* ATCC CI is spherical in shape with the average diameter of 0.79 µm ($n = 15$, $SD = 0.05$). After treatment with A16 (0.25 µg/mL), *S. aureus* ATCC CI cells became large with the average diameter of 2.41 µm ($n = 15$, $SD = 0.49$) (Fig. 5 (E) and 5 (F)). The above results confirm that A16 interferes with the normal function of FtsZ, further leads to improper cell division and finally causes bacterial cell death.

3.5. Stimulation of FtsZ polymerization dynamics

In-depth studies on the dynamic of FtsZ protein have shown that some FtsZ-targeting agents can stimulate FtsZ polymerization dynamics and stabilize FtsZ polymeric structures, which contribute to the antibacterial activity of FtsZ inhibitors.^{21,22} Therefore, the polymerization

assay of *B. subtilis* FtsZ (BsFtsZ) at different concentrations of A16 were performed utilizing a microplate reader at 340 nm (A_{340}). The time-dependent A_{340} profiles illustrated in Fig. 6(A) indicates that A16 increases the kinetics of BsFtsZ polymerization, with the magnitude of stimulatory effect in a concentration-dependent manner. As expected, neither CIP, LIN nor vehicle impacted the polymerization of BsFtsZ to any significant degree. Fig. 6(B) shows that A16-S possesses a stronger impact than A16-R and A16 on the FtsZ polymerization, which is correlated with its antibacterial activity. In contrast, A26_{pre} displays a much weaker stimulatory effect than A16 at the same concentration, which tallies with its antibacterial activity as well.

3.6. Stability of A16 in mouse plasma in vitro

To evaluate the primary pharmacokinetic profile of A16, the time-dependent stability of A16 in the mouse plasma at 37 °C was assessed *in vitro*. The data of liquid chromatography-tandem mass spectrometry

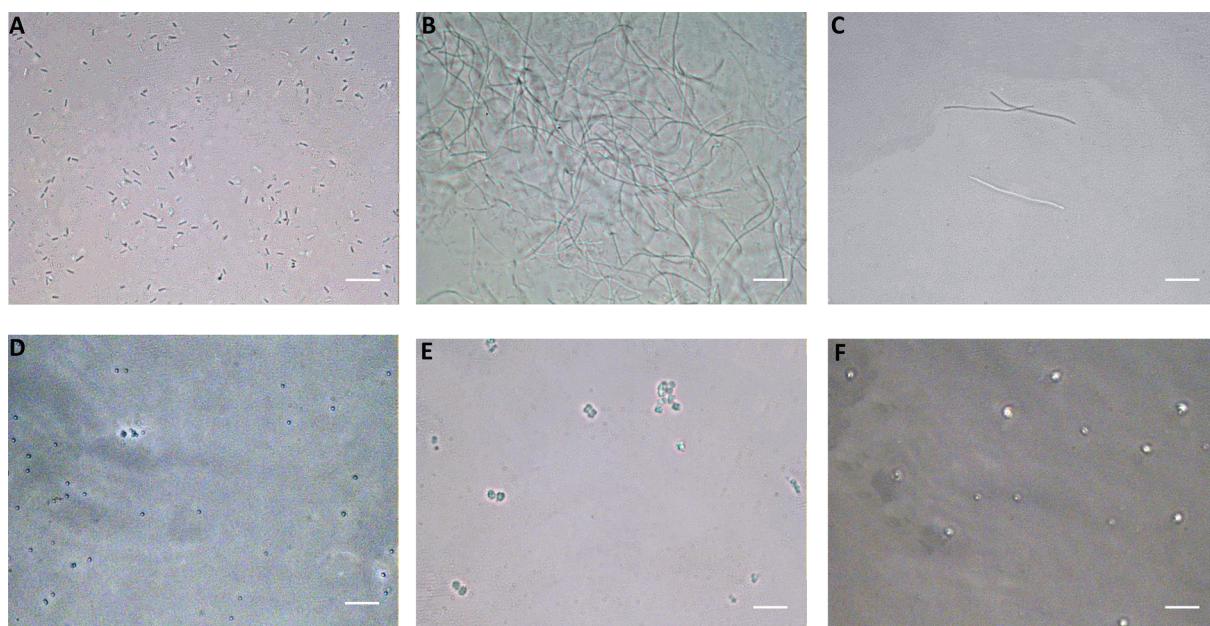


Fig. 5. Effects of compound A16 on the bacterial cell morphology. *B. subtilis* cells were grown in the absence (A) or in the presence (B and C) of A16 at 0.25 µg/mL. *S. aureus* CI cells were grown in the absence (D) or in the presence (E and F) of A16 at 0.25 µg/mL. Scale Bar = 10 µm.

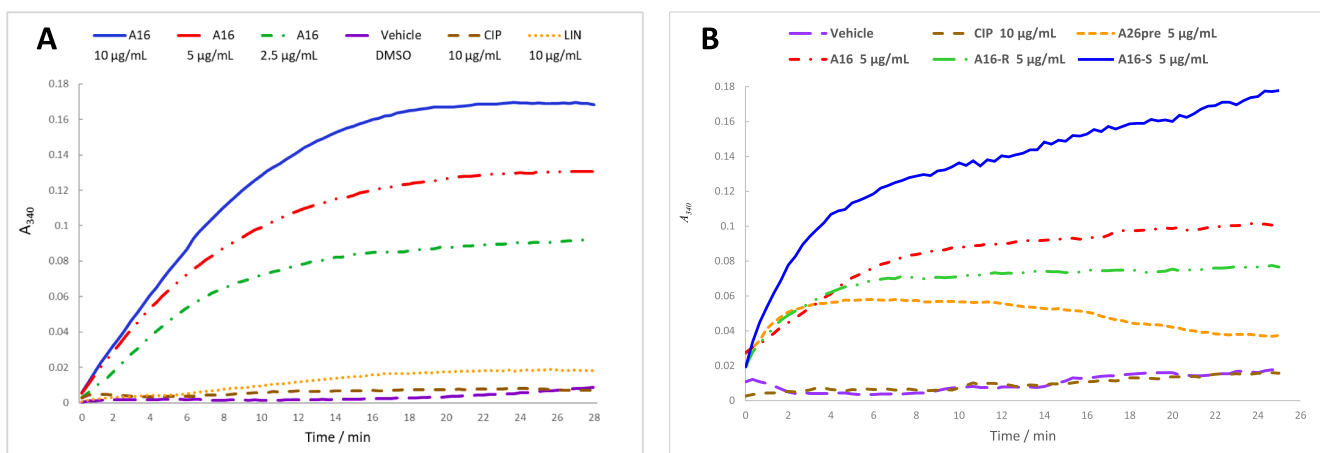


Fig. 6. The impact of **A16** on the polymerization of BsFtsZ. (A) Effect on the polymerization of FtsZ in the absence or presence of **A16** at the concentration of 2.5, 5 and 10 µg/mL. CIP and LIN were included as negative (non-FtsZ-targeting) controls. (B) Effect on the polymerization of FtsZ in the absence or in the presence of 5 µg/mL of compound **A26_{pre}**, **A16**, **A16-R** and **A16-S**.

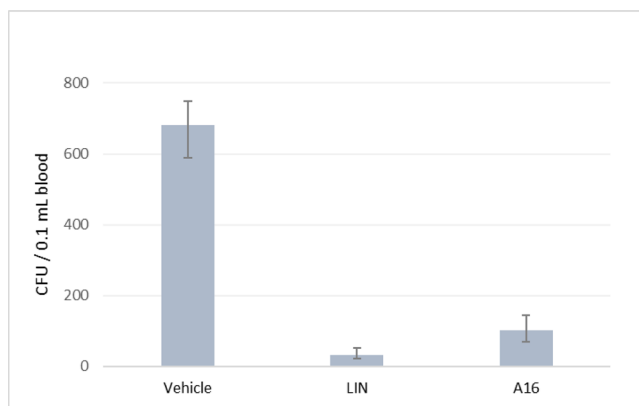


Fig. 7. Efficacy of **A16** in mouse model of blood infection with *S. aureus*. The CFU numbers of 0.1 mL blood were recorded and LIN was included as a positive control.

(LC-MS) demonstrated an almost constant peak area, which corresponded with the molecular mass of **A16**. The above results revealed that **A16** did not get oxidized to the corresponding isoxazole product and remained basically undegraded in the mouse plasma over 24 h, which indicates its excellent chemical stability in plasma (Supplementary data, Figs. S4-S13).

3.7. *In vivo* efficacy against *S. aureus* (MDRS) in mouse model

Three groups of mice were inoculated with 8.5×10^8 CFU clinical isolated *S. aureus* which is resistant to CIP and ERY through tail vein injection. Then the infected mice were administered with vehicle, LIN and **A16**, respectively, in a dose of 10 mg/kg each time and three times a day through tail vein injection. After two days, the bacterial CFU (colony-forming units) of blood collected from retro-orbital plexus was recorded.^{12,23} Fig. 7 displays that LIN and **A16** at same doses both can significantly decrease the bacterial burden in blood. Note that, even having superior efficacy *in vitro* and time-kill kinetics, **A16** still did not work better *in vivo* than LIN, which could be due to its inadequate pharmacokinetic properties.

3.8. Cytotoxicity of **A16** to mammalian cells

To evaluate any potential toxicity against mammalian cell, a 48 h MTT-based assay was performed to assess the cytotoxicity of **A16** to Hela cells.¹⁵ This compound was proved to be minimally toxic to Hela

cells, with a 50% inhibitory concentration (IC_{50}) of > 64 µg/mL which is much higher than its antibacterial MIC values. Albeit testing a single mammalian cell line, based on this initial result obtained we found that **A16** was associated with a significant therapeutic window. Further studies on additional mammalian and human cell lines will be directed toward assessing the general nature of this result.

3.9. The docking analysis of **A16**, **B13** and **A26_{pre}** with FtsZ

Docking study was undertaken to rationalize the observed antibacterial activity and investigate the interactions of the representative compounds with the FtsZ binding site. The docking analysis of **A16**, **B13** and **A26_{pre}** were explored and contrasted utilizing a reported crystal structure of SaFtsZ (PDB code: 3vob)²⁴ and Ledock. The docking results are shown in Fig. 8. Both **A16**, **B13** and **A26_{pre}** were well combined with FtsZ protein. The molecular conformations of **A16**, **A26_{pre}** and **PC190723** almost overlapped with each other (Fig. 8A), which indicate that the binding site of **A16** is in good agreement with **PC190723**. Their three pharmacophores of **A16** are connected by the middle O–C bond, and the whole molecule presents an M-shaped conformation (Fig. 8A).¹⁵ The benzamide moiety of the above three compounds forms the same hydrogen bonds and ion–dipole forces with the surrounding amino acid residues Asn263, Thr296, Asn208 and Leu209, as well as Ca^{2+} , which are critical forces to grasp the FtsZ protein. The series-connected heterocycle on the right extends into a hydrophobic cavity. Comparing the docking conformations of **A16** and **B13** (Fig. 8C and 8D), a conventional hydrogen bonding interaction was predicted between the oxygen atom in the 4,5-dihydroisoxazole of **A16** and Gly196. Besides, **A16** could also form hydrogen-bonding interaction with a water molecule, while **B13** lacked the above two interactions. Consequently, this little conformational change caused an additional affinity of **A16** for FtsZ protein, and further increased stimulatory effect on FtsZ polymerization, thereby leading to the enhanced antibacterial activity.

3.10. Discussion of structure-activity relationships (SARs)

Detailed SARs analysis on series A is summarized to reveal different substituents that are crucial to maintaining the antibacterial activity. Firstly, **A3-A8** with halogen substitutions exhibited stronger activity than **A1** without substitution on the benzene ring, exhibiting a 2–8 fold increase in antibacterial activity against *B. subtilis* ATCC9372. Similarly, they also showed increased activity against *B. pumilus* CMCC63202 with the MIC values of 2–8 µg/mL, which was 8–32 fold more potent than that of **A1**. It is suggested that the introduction of halogen atoms on the

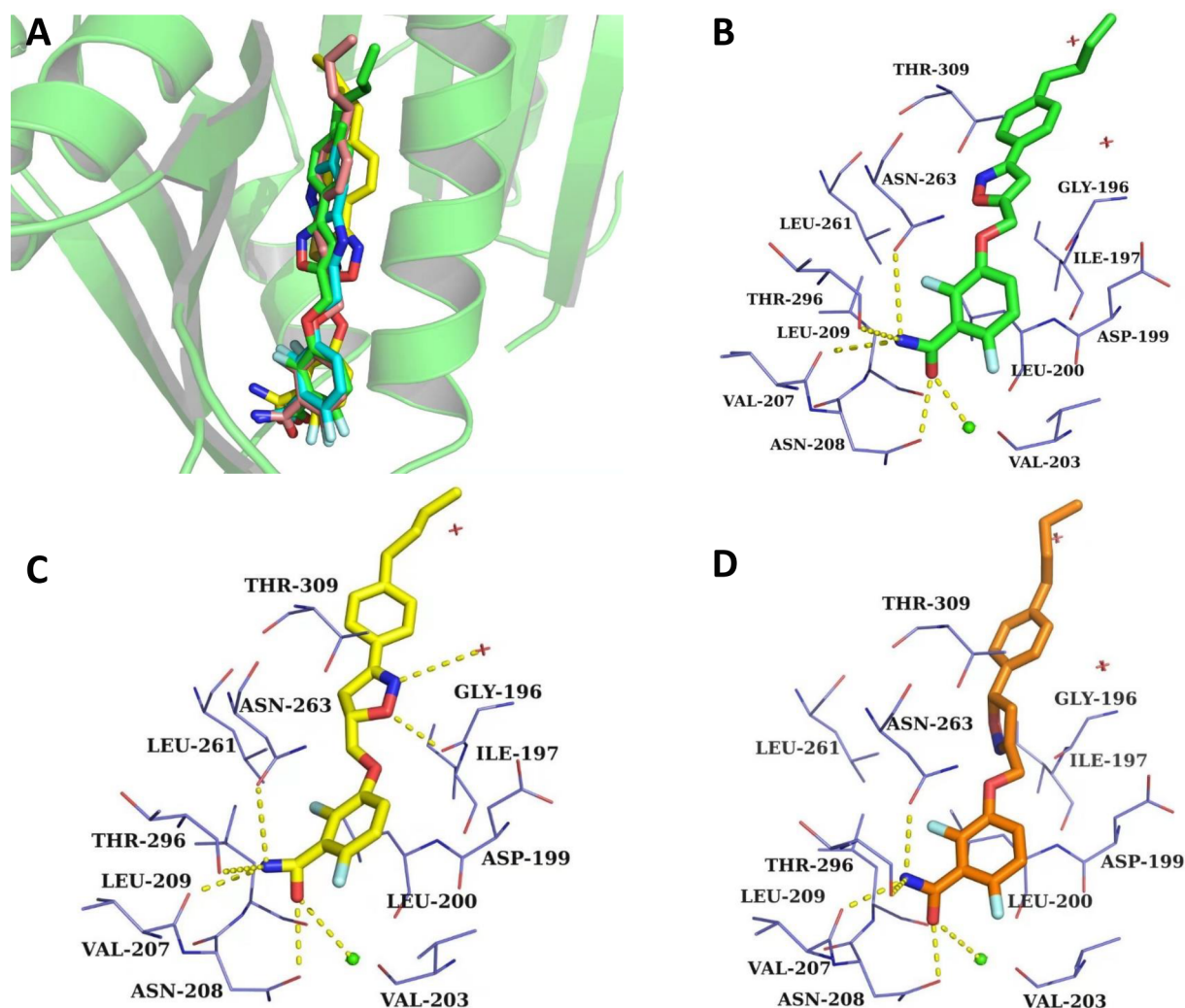


Fig. 8. Predicted binding modes of SaFtsZ (PDB ID: 3vob) in complex with **A16**, **B13** and **26_{pre}**. (A) The predicted binding models of **A16** (yellow structure), **A26_{pre}** (green structure) and **PC190723** (cyan structure); (B) The predicted binding models of **A26_{pre}**; (C) The predicted binding model of **A16**; (D) The predicted binding models of **B13** (brown structure).

benzene ring is beneficial to enhance the antibacterial activity of compounds. We infer that the conjugation of halogen atoms may increase the lipid solubility of compounds and facilitate their penetration through bacterial cell membranes, thereby enhancing their antibacterial activity. Secondly, the antibacterial activity of the most compounds in **A11-A26** was significantly better than that of **A1** when tested against *B. subtilis* ATCC9372 and *B. pumilus* CMCC63202. **A14-A17** generated potent activity, which was superior or equivalent to controls (PC, CIP, LIN and ERY). The tested results also show that the antibacterial activity of the compounds is enhanced when the electron-donating groups are attached to the benzene ring. We speculate that the electron-rich substituted benzene rings may produce π - π stacking and hydrophobic interactions with the surrounding amino acid residues in the hydrophobic cavity of FtsZ. Besides, the length of alkyl substitution on the benzene ring has a significant influence on the antibacterial activity as well. Increasing the length of the alkyl group on the benzene ring (**A11** to **A17**) leads to enhanced antibacterial activity. When possessing the *n*-butyl group (**A16**), the activity reaches a peak value, while the further elongation of the alkyl side chain (**A17**) decreases the activity dramatically. This may be well explained by the fact that the binding pocket of FtsZ for these compounds has a volume restriction. For **A19-A25**, their antibacterial activity gradually increased with the extension of the alkoxy side chain, which demonstrates the same trend as **A11-A17** in antibacterial activity. Thirdly, the position of substituent

on the phenyl ring plays a crucial role in the antibacterial potency. For example, varying the position of chlorine atom from *para*-position (**A4**) to *ortho*-position (**A2**) sharply decrease the antibacterial activity. Replacing the *para*-methoxy group (**A21**) by an *ortho*-methoxy group (**A19**) directly leads to the loss of antibacterial activity. It is possible that *para*-substituent with appropriate length and flexibility is more suitable for the narrow hydrophobic slit of FtsZ. Taken together, when aliphatic alkane was introduced to the *para*-position of the benzene ring, the contribution of antibacterial activity was significantly stronger than that of other substituents. The representative compound **A16** offered the most potent and balanced activity against all the tested Gram-positive bacteria (MIC = 0.125–4 μ g/mL).

In series B, **B1-B7** had different halogen atoms on the benzene ring. Among them, the antibacterial activity of **B3** and **B4** was stronger than that of **B1-B2** and **B5-B7**, which can be inferred that the contribution of halogen atom for activity is Cl > Br > F, and chlorine atom at the C-2 and C-4 position of the phenyl ring offered the most potent antibacterial activity. By comparing the structures of **B8-B13**, increasing the length of the alkyl side chain was found to improve the antibacterial activity greatly. This may be explained that the long-chain aliphatic alkanes have flexibility, which are allowed to enter the hydrophobic cavity and bind with amino acid residues. As for **B14-B18** that possess different length alkoxy groups on the benzene ring, shortening the length of the alkoxy group significantly weakened their antibacterial activity, which

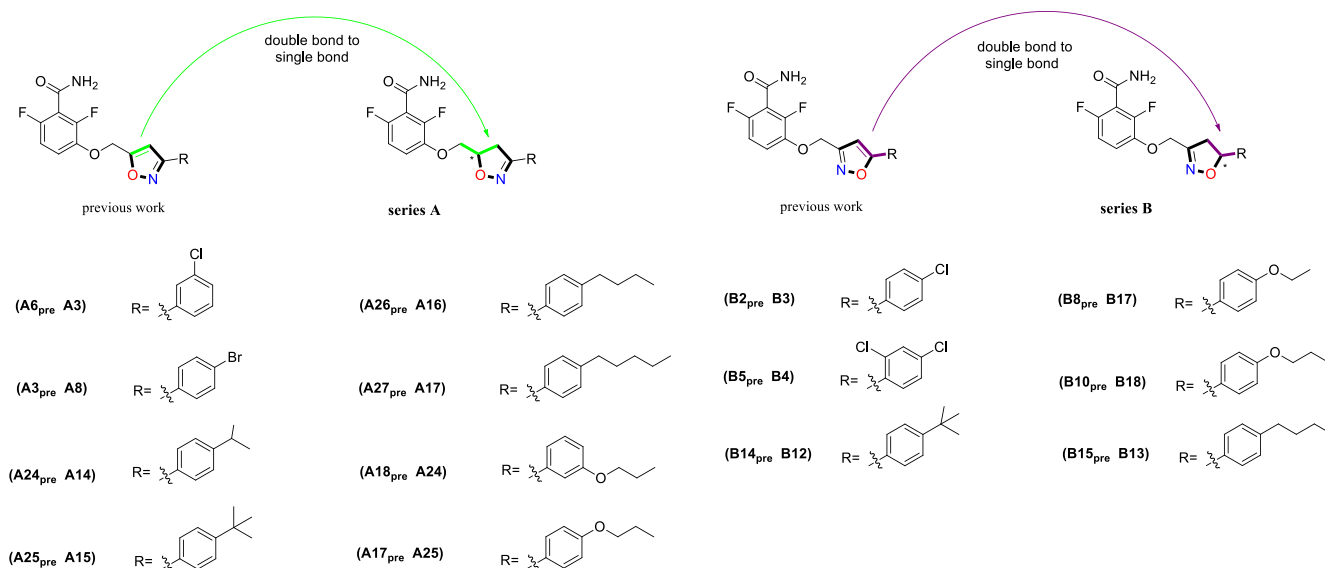


Fig. 9. The structures of the selected compounds used for comparison from our present and previous studies.

are similar to that of **B8-B13**. Besides, altering the position of chlorine atom from *para*-position (**B3**) to *ortho*-position (**B1**) or *meta*-position (**B2**) sharply decreased the antibacterial activity. Similarly, replacing the *para*-ethoxy group (**B17**) with an *ortho*-ethoxy group (**B15**) or *meta*-ethoxy substitution (**B16**) also weakened the antibacterial activity. Thus, we can conclude that the extension direction of the side chain on the benzene ring in space has a significant effect on the antibacterial activity. In short, aliphatic alkanes on *para*-position of the benzene rings exert more potent antibacterial activity than those on other positions. The representative compound **B13** with the *n*-butyl group exhibited excellent antibacterial activity against *B. subtilis* ATCC9372 and *B. pumilus* CMCC63202 with the MIC values of ≤ 0.125 and $0.5 \mu\text{g/mL}$, respectively.

In general, the structures of the series A and series B almost overlap with each other, and their structural difference lies in the 4,5-dihydroisoxazole. From the MIC results, **A11-A16** have much better antibacterial activity than **B8-B13**, but these compounds possess the same warhead of 2,6-difluorobenzamide and the same tail of the substituted benzene ring. The only difference in their structure is connections of the 4,5-dihydroisoxazole ring, which interfere with the potency of their antibacterial activity. Also, **A19-A25** with alkoxy side chains on the benzene rings are structurally similar to **B14-B18** but exhibit stronger antibacterial activity. Thus, it is concluded that the 4,5-dihydroisoxazole ring in the structure has a positive effect on the antibacterial activity and the relative position of heteroatoms in the 4,5-dihydroisoxazole ring may have a direct influence on the interaction with FtsZ binding pocket, which was confirmed by the docking results. The oxygen atom on the 4,5-dihydroisoxazole of the series A is adjacent to Gly196 and a water molecule, tending to interact with each other. The subtle differences in heteroatom positions on the 4,5-dihydroisoxazole alter the binding affinity of compounds to FtsZ target, which explain the significant differences in antibacterial activity between series A and series B.

A16 has the most promising antibacterial activity among all tested compounds, while **B14_{pre}** (Fig. 9) is the best compound that was screened from our previous work.¹⁶ For all that, **A16** still displays 4-, 8- and 8-fold more potent antibacterial activity against *S. aureus* ATCC25923, *S. aureus* ATCC43300 and *S. aureus* PR than **B14_{pre}**. Moreover, this compound also exhibits excellent activity against *B. pumilus* CMCC63202, comparable to **B14_{pre}**. This indicates that 4,5-dihydroisoxazol-containing benzamide derivatives demonstrate increased antibacterial activity, compared with our reported 4,5-isoxazol-containing benzamide derivatives.¹⁶ Not only that, 4,5-

dihydroisoxazol-containing benzamide derivatives also show broad antibacterial spectrum, and are more active against *S. aureus* strain. For example, the antibacterial activity of **A14**, **A15**, **A16**, **A17** and **A24** against *B. pumilus* CMCC63202 were at least 2-fold more active than **A24_{pre}**, **A25_{pre}**, **A26_{pre}**, **A27_{pre}** and **A18_{pre}** (Fig. 9), respectively. In particular, **A16** has not only significantly improved activity against *S. aureus* ATCC25923, which is 128-fold more active than **A26_{pre}**, but also remarkably inhibits the growth of *S. aureus* PR, which is a 128-fold improvement compared with **A26_{pre}**. It is unexpected that **A14** and **A15** exhibit 2- to 16-fold better activity against *S. aureus* than **A24_{pre}** and **A25_{pre}**. Besides, **A3**, **A8**, **A24** and **A25** exhibited moderate antibacterial activity against the tested Gram-positive bacteria with the MIC values of 2–32 $\mu\text{g/mL}$. In contrast, the corresponding **A6_{pre}**, **A3_{pre}**, **A18_{pre}** and **A17_{pre}** were inactive against the above tested strains except for *B. subtilis* ATCC9372. As for series B, **B3**, **B17** and **B18** exert better activity against *B. subtilis* ATCC9372 and *B. pumilus* CMCC63202, while the corresponding **B2_{pre}**, **B8_{pre}** and **B10_{pre}** (Fig. 9) have no obvious antibacterial activity. Moreover, **B4** and **B13** show a broad spectrum activity, but the corresponding **B5_{pre}** and **B15_{pre}** (Fig. 9) barely inhibit the growth of *B. subtilis* ATCC9372.

Although there is little change in their structure, the antibacterial activity is greatly improved, and the antibacterial spectrum has been broadened. Thus, we can conclude that the replacement of the isoxazole ring with a 4,5-dihydroisoxazole ring produces a positive influence on antibacterial activity. Based on stereochemistry of **A16** and **A26_{pre}**, the 4,5-dihydroisoxazole ring in molecular structure has some flexibility and can be twisted to suit the hydrophobic cavity of FtsZ. In contrast, the isoxazole ring in molecular structure is rigid and limits its distortion to accommodate hydrophobic cavity, which was confirmed by the docking results (Fig. 8B and 8C). Also, lipid/water partition coefficients ($\log P$) as one of the most important factors have been extensively employed to predict the bioactivity of target molecules.²⁵ Therefore, we theoretically calculated the $\log P$ values (ClogP) of **A16** and **A26_{pre}** molecules by the commercial ChemBioOffice 2010 (Cambridge Soft, USA) to further confirm their influence on antibacterial activity. Results showed that the ClogP values of **A16** and **A26_{pre}** are 4.18 and 4.19, respectively, which don't affect their antibacterial activity. Taken together, the replacement of the isoxazole ring in molecular structure with a 4,5-dihydroisoxazole ring leads to the change of spatial configuration of the target compound. It suits the hydrophobic cavity of FtsZ, thereby strengthening affinity for FtsZ, which is consistent with our design strategy.

4. Conclusion

Using the structure-based optimization strategy, two series of 4,5-dihydroisoxazol-5-yl- and 4,5-dihydroisoxazol-3-yl-containing benzamide derivatives were designed, synthesized, and tested for their *in vitro* and *in vivo* biological activities. They were pharmacologically evaluated as FtsZ-targeting antibacterial agents as well. The results indicated that several compounds exhibited significant antibacterial activity against most of the tested strains, including the multidrug-resistant strains. It is noteworthy that **A16** display significantly activity against three resistant strains of methicillin-resistant, penicillin-resistant and clinical isolated *S. aureus*, and a sensitive strain of *S. aureus* with the MIC values ranging from 0.25 to 0.5 µg/mL, which are comparable to those observed with PC190723 and LIN, and are much better than that of CLA. It is worth noting that substituting a 4,5-dihydroisoxazole ring for the isoxazole ring resulted in a great increase in antibacterial activity and the broadening of antibacterial spectrum. Regarded as a whole, the research findings described herein highlight **A16** as a lead compound with potent bactericidal activity and reinforce the importance of FtsZ as a promising antibacterial target. Further optimization of the 4,5-dihydroisoxazol-5-yl-containing benzamide derivatives is ongoing in our lab.

5. Experimental section

5.1. General experimental protocol

All commercially available chemicals and reagents were used without any further purification unless otherwise indicated. Reactions progress was monitored by thin-layer chromatography (TLC) on 0.25-mm pre-coated silica GF254 plates. Flash column chromatography was carried out with the indicated solvents using silica gel 200–300 mesh size. ¹H NMR spectra were recorded at 400 or 600 MHz, and ¹³C NMR spectra were recorded at 150 MHz in ppm using appropriate deuterated solvents. Mass spectra were obtained on the API 4000 instrument. HRMS were measured using an Orbitrap analyzer. Melting points were determined using a RY-1 melting point apparatus without corrected. ECD spectra were performed on a Chirascan spectropolarimeter. Analytical HPLC was carried out on an Agilent 1200 Series equipment coupled to ultraviolet-visible detector (UVD) at 254 nm with a Diamonil C18 reversed phase column (150 × 4.6 mm, 5 µm) at ambient temperature. The effective chromatogram was obtained using the mobile phase of methanol: water (60 : 40, vol./vol.) at the flow rate of 1.0 mL/min. The purity of the tested compounds as determined by analytical HPLC was more than 95%. Compounds **4**, **5**, **6** and **9** were synthesized according to our previous reports.¹⁶ The detailed synthetic methods of series **A** and **B** refer to the [Supplementary data](#).

5.2. Typical compounds of the series A

5.2.1. 2,6-Difluoro-3-((3-phenyl-4,5-dihydroisoxazol-5-yl)methoxy)benzamide (**A1**)

White solid, Mp: 148–150 °C; ¹H NMR (400 MHz, DMSO-*d*₆) δ 8.11 (s, 1H), 7.83 (s, 1H), 7.73–7.66 (m, 2H), 7.51–7.44 (m, 3H), 7.26 (td, *J* = 9.3, 5.2 Hz, 1H), 7.07 (td, *J* = 8.9, 1.9 Hz, 1H), 5.13–5.03 (m, 1H), 4.28–4.14 (m, 2H), 3.61 (dd, 1H), 3.32–3.25 (m, 1H). ¹³C NMR (150 MHz, DMSO-*d*₆) δ 161.77, 157.03, 152.51 (dd, *J*_{F-C} = 241.2, 6.6 Hz), 148.39 (dd, *J*_{F-C} = 248.7, 8.4 Hz), 143.38 (dd, *J*_{F-C} = 11.0, 3.2 Hz), 130.60, 129.70, 129.30, 127.09, 117.08 (dd, *J*_{F-C} = 24.9, 20.4 Hz), 116.32 (dd, *J*_{F-C} = 9.4, 2.2 Hz), 111.44 (dd, *J*_{F-C} = 23.0, 3.8 Hz), 79.09, 71.37, 37.02. HRMS (ESI) calcd for C₁₇H₁₅F₂N₂O₃ [M + H]⁺, 333.1045, found 333.1044.

5.2.2. 2,6-Difluoro-3-((3-(2-chlorophenyl)-4,5-dihydroisoxazol-5-yl)methoxy)benzamide (**A2**)

White solid, Mp: 130–132 °C; ¹H NMR (600 MHz, Chloroform-*d*) δ 7.66–7.61 (m, 1H), 7.46–7.42 (m, 1H), 7.39–7.35 (m, 1H), 7.34–7.30

(m, 1H), 7.11 (td, *J* = 9.1, 5.1 Hz, 1H), 6.90 (td, *J* = 9.1, 2.0 Hz, 1H), 5.94 (d, *J* = 44.1 Hz, 2H), 5.16–5.10 (m, 1H), 4.24–4.17 (m, 2H), 3.74–3.52 (m, 2H). ¹³C NMR (150 MHz, DMSO-*d*₆) δ 161.77, 156.37, 152.51 (dd, *J*_{F-C} = 241.6, 6.7 Hz), 148.38 (dd, *J*_{F-C} = 248.7, 8.6 Hz), 143.38 (dd, *J*_{F-C} = 10.6, 3.3 Hz), 132.11, 131.78, 131.22, 130.96, 129.04, 127.94, 117.11 (dd, *J*_{F-C} = 25.0, 20.3 Hz), 116.20 (dd, *J*_{F-C} = 9.3, 2.3 Hz), 111.43 (dd, *J*_{F-C} = 23.1, 3.8 Hz), 79.30, 71.16, 39.45. ESI-MS calcd for C₁₇H₁₄ClF₂N₂O₃ [M + H]⁺, 367.1, found 367.2.

5.2.3. 2,6-Difluoro-3-((3-(3-chlorophenyl)-4,5-dihydroisoxazol-5-yl)methoxy)benzamide (**A3**)

White solid, Mp: 144–146 °C; ¹H NMR (400 MHz, DMSO-*d*₆) δ 8.11 (s, 1H), 7.83 (s, 1H), 7.74–7.63 (m, 2H), 7.58–7.46 (m, 2H), 7.25 (td, *J* = 9.3, 5.2 Hz, 1H), 7.08 (td, *J* = 9.0, 1.9 Hz, 1H), 5.16–5.06 (m, 1H), 4.27–4.14 (m, 2H), 3.61 (dd, *J* = 17.2, 11.1 Hz, 1H), 3.39–3.32 (m, 1H). ¹³C NMR (150 MHz, DMSO-*d*₆) δ 161.73, 156.28, 152.52 (dd, *J*_{F-C} = 241.3, 6.6 Hz), 148.39 (dd, *J*_{F-C} = 248.7, 8.4 Hz), 143.35 (dd, *J*_{F-C} = 11.0, 3.2 Hz), 134.04, 131.80, 131.22, 130.36, 126.67, 125.72, 117.09 (dd, *J*_{F-C} = 24.9, 20.4 Hz), 116.32 (dd, *J*_{F-C} = 9.4, 2.3 Hz), 111.44 (dd, *J*_{F-C} = 23.1, 3.9 Hz), 79.53, 71.30, 36.77. ESI-MS calcd for C₁₇H₁₄ClF₂N₂O₃ [M + H]⁺, 367.1, found 367.2.

5.2.4. 2,6-Difluoro-3-((3-(4-chlorophenyl)-4,5-dihydroisoxazol-5-yl)methoxy)benzamide (**A4**)

White solid, Mp: 146–147 °C; ¹H NMR (600 MHz, DMSO-*d*₆) δ 8.11 (s, 1H), 7.82 (s, 1H), 7.71 (d, *J* = 8.6 Hz, 2H), 7.54 (d, *J* = 8.6 Hz, 2H), 7.25 (td, *J* = 9.3, 5.2 Hz, 1H), 7.07 (td, *J* = 8.8, 1.8 Hz, 1H), 5.13–5.06 (m, 1H), 4.26–4.16 (m, 2H), 3.64–3.56 (m, 1H), 3.31–3.26 (m, 1H). ¹³C NMR (150 MHz, DMSO-*d*₆) δ 161.71, 156.29, 152.51 (dd, *J*_{F-C} = 240.1, 9.8 Hz), 148.38 (dd, *J*_{F-C} = 247.6, 11.3 Hz), 143.31 (dd, *J*_{F-C} = 13.6, 3.8 Hz), 135.16, 129.40, 128.85, 128.61, 117.08 (dd, *J*_{F-C} = 25.7, 19.6 Hz), 116.36 (d, *J*_{F-C} = 15.1 Hz), 111.51 (dd, *J*_{F-C} = 22.7, 5.3 Hz), 79.42, 71.31, 36.87. ESI-MS calcd for C₁₇H₁₄ClF₂N₂O₃ [M + H]⁺, 367.1, found 367.3.

5.2.5. 2,6-Difluoro-3-((3-(2,4-dichlorophenyl)-4,5-dihydroisoxazol-5-yl)methoxy)benzamide (**A5**)

White solid, Mp: 103–104 °C; ¹H NMR (600 MHz, DMSO-*d*₆) δ 8.12 (s, 1H), 7.83 (s, 1H), 7.77 (d, *J* = 2.1 Hz, 1H), 7.66 (d, *J* = 8.4 Hz, 1H), 7.55 (dd, *J* = 8.4, 2.1 Hz, 1H), 7.26 (td, *J* = 9.3, 5.2 Hz, 1H), 7.08 (td, *J* = 9.0, 1.8 Hz, 1H), 5.16–5.09 (m, 1H), 4.27–4.16 (m, 2H), 3.68 (dd, *J* = 17.2, 11.0 Hz, 1H), 3.38 (dd, *J* = 17.3, 7.0 Hz, 1H). ¹³C NMR (150 MHz, DMSO-*d*₆) δ 161.73, 155.63, 152.50 (dd, *J*_{F-C} = 241.5, 6.7 Hz), 148.36 (dd, *J*_{F-C} = 248.8, 8.3 Hz), 143.35 (dd, *J*_{F-C} = 10.8, 3.1 Hz), 135.55, 133.14, 132.44, 130.53, 128.20, 128.02, 117.11 (dd, *J*_{F-C} = 25.0, 20.5 Hz), 116.21 (d, *J*_{F-C} = 9.5 Hz), 111.43 (dd, *J*_{F-C} = 22.8, 3.8 Hz), 79.49, 71.12, 39.21. ESI-MS calcd for C₁₇H₁₆Cl₂F₂N₂O₃ [M + NH₄]⁺, 418.1, found 418.5.

5.2.6. 2,6-Difluoro-3-((3-(3,4-dichlorophenyl)-4,5-dihydroisoxazol-5-yl)methoxy)benzamide (**A6**)

White solid, Mp: 181–182 °C; ¹H NMR (400 MHz, DMSO-*d*₆) δ 8.12 (s, 1H), 7.90 (d, *J* = 1.8 Hz, 1H), 7.84 (s, 1H), 7.75 (d, *J* = 8.4 Hz, 1H), 7.69 (dd, *J* = 8.5, 1.9 Hz, 1H), 7.25 (td, *J* = 9.3, 5.2 Hz, 1H), 7.08 (td, *J* = 9.0, 1.9 Hz, 1H), 5.18–5.08 (m, 1H), 4.26–4.15 (m, 2H), 3.66–3.56 (m, 1H), 3.38–3.34 (m, 1H). ¹³C NMR (150 MHz, DMSO-*d*₆) δ 161.70, 155.72, 152.52 (dd, *J*_{F-C} = 241.6, 6.6 Hz), 148.38 (dd, *J*_{F-C} = 248.6, 8.4 Hz), 143.33 (dd, *J*_{F-C} = 10.9, 3.1 Hz), 133.04, 132.16, 131.57, 130.38, 128.83, 127.10, 117.10 (dd, *J*_{F-C} = 25.0, 20.4 Hz), 116.33 (d, *J*_{F-C} = 9.4 Hz), 111.44 (dd, *J*_{F-C} = 22.7, 3.8 Hz), 79.80, 71.25, 36.67. ESI-MS calcd for C₁₇H₁₃Cl₂F₂N₂O₃ [M + H]⁺, 401.0, found 401.2.

5.2.7. 2,6-Difluoro-3-((3-(4-fluorophenyl)-4,5-dihydroisoxazol-5-yl)methoxy)benzamide (**A7**)

White solid, Mp: 155–156 °C; ¹H NMR (600 MHz, Chloroform-*d*) δ 7.71–7.66 (m, 2H), 7.14–7.07 (m, 3H), 6.89 (td, *J* = 9.1, 2.0 Hz, 1H),

5.91 (d, $J = 52.1$ Hz, 2H), 5.13 – 5.07 (m, 1H), 4.26–4.13 (m, 2H), 3.56–3.38 (m, 2H). ^{13}C NMR (150 MHz, DMSO- d_6) δ 164.34, 162.70, 161.74, 156.20, 152.51 (dd, $J_{F-C} = 241.5$, 6.6 Hz), 148.38 (dd, $J_{F-C} = 248.5$, 8.4 Hz), 143.36 (dd, $J_{F-C} = 10.9$, 3.2 Hz), 129.41 (d, $J_{F-C} = 8.6$ Hz), 126.33 (d, $J_{F-C} = 3.2$ Hz), 117.09 (dd, $J_{F-C} = 25.0$, 20.4 Hz), 116.35 (d, $J_{F-C} = 21.9$ Hz), 111.43 (dd, $J_{F-C} = 23.1$, 3.8 Hz), 79.22, 71.33, 37.11. ESI-MS calcd for $\text{C}_{17}\text{H}_{14}\text{F}_3\text{N}_2\text{O}_3$ [M+H] $^+$, 351.3, found 351.4.

5.2.8. 2,6-Difluoro-3-((3-(4-bromophenyl)-4,5-dihydroisoxazol-5-yl)methoxy)benzamide (A8)

White solid, Mp: 144–146 °C; ^1H NMR (600 MHz, Chloroform- d) δ 7.55 (s, 4H), 7.09 (td, $J = 9.1$, 5.1 Hz, 1H), 6.89 (td, $J = 9.1$, 2.0 Hz, 1H), 5.92 (d, 2H), 5.14–5.08 (m, 1H), 4.24–4.13 (m, 2H), 3.54–3.37 (m, 2H). ^{13}C NMR (150 MHz, DMSO- d_6) δ 161.72, 156.40, 152.51 (dd, $J_{F-C} = 241.4$, 6.7 Hz), 148.38 (dd, $J_{F-C} = 248.7$, 8.5 Hz), 143.35 (dd, $J_{F-C} = 10.7$, 3.2 Hz), 132.30, 129.05, 123.91, 117.09 (dd, $J_{F-C} = 24.9$, 20.4 Hz), 116.31 (dd, $J_{F-C} = 9.8$, 2.3 Hz), 111.43 (dd, $J_{F-C} = 22.8$, 3.9 Hz), 79.44, 71.31, 36.81. ESI-MS calcd for $\text{C}_{17}\text{H}_{14}\text{BrF}_2\text{N}_2\text{O}_3$ [M+H] $^+$, 411.0, found 411.2.

5.2.9. 2,6-Difluoro-3-((3-(4(dimethylamino)phenyl)-4,5-dihydroisoxazol-5-yl)methoxy)benzamide (A9)

White solid, Mp: 217–219 °C; ^1H NMR (600 MHz, DMSO- d_6) δ 8.12 (s, 1H), 7.84 (s, 1H), 7.50 (d, $J = 8.9$ Hz, 2H), 7.26 (td, $J = 9.3$, 5.1 Hz, 1H), 7.08 (td, $J = 9.0$, 1.8 Hz, 1H), 6.75 (d, $J = 8.8$ Hz, 2H), 5.02–4.94 (m, 1H), 4.23–4.12 (m, 2H), 3.52 (dd, $J = 16.8$, 10.8 Hz, 1H), 3.24 (dd, $J = 16.9$, 7.3 Hz, 1H), 2.96 (s, 6H). ^{13}C NMR (150 MHz, DMSO- d_6) δ 161.74, 156.66, 153.26 (d, $J_{F-C} = 6.3$ Hz), 151.77, 151.66 (d, $J_{F-C} = 6.7$ Hz), 148.36 (dd, $J_{F-C} = 248.7$, 8.2 Hz), 143.41 (dd, $J_{F-C} = 11.4$, 2.6 Hz), 128.21, 117.08 (dd, $J_{F-C} = 24.8$, 20.5 Hz), 116.74, 116.29 (d, $J_{F-C} = 9.1$ Hz), 112.15, 111.42 (dd, $J_{F-C} = 23.2$, 3.7 Hz), 78.21, 71.43, 37.49, 26.82, 25.85. ESI-MS calcd for $\text{C}_{19}\text{H}_{20}\text{F}_2\text{N}_3\text{O}_3$ [M+H] $^+$, 376.4, found 376.4.

5.2.10. 2,6-Difluoro-3-((3-(4-cyanophenyl)-4,5-dihydroisoxazol-5-yl)methoxy)benzamide (A10)

White solid, Mp: 156–158 °C; ^1H NMR (600 MHz, Chloroform- d) δ 7.79 (d, $J = 8.5$ Hz, 2H), 7.71 (d, $J = 8.6$ Hz, 2H), 7.09 (td, $J = 9.0$, 5.1 Hz, 1H), 6.89 (td, $J = 9.1$, 2.0 Hz, 1H), 5.90 (d, $J = 52.2$ Hz, 2H), 5.20 – 5.13 (m, 1H), 4.26–4.18 (m, 2H), 3.56–3.42 (m, 2H). ^{13}C NMR (150 MHz, DMSO- d_6) δ 161.69, 156.41, 152.50 (dd, $J_{F-C} = 241.5$, 6.6 Hz), 148.36 (dd, $J_{F-C} = 248.7$, 8.4 Hz), 143.31 (dd, $J_{F-C} = 11.2$, 3.0 Hz), 134.06, 133.23, 127.79, 118.95, 117.08 (dd, $J_{F-C} = 25.2$, 20.3 Hz), 116.31 (d, $J_{F-C} = 8.9$ Hz), 112.74, 111.43 (dd, $J_{F-C} = 23.1$, 3.8 Hz), 79.99, 71.26, 36.45. ESI-MS calcd for $\text{C}_{18}\text{H}_{14}\text{F}_2\text{N}_3\text{O}_3$ [M+H] $^+$, 358.3, found 358.2.

5.2.11. 2,6-Difluoro-3-((3-(*m*-tolyl)-4,5-dihydroisoxazol-5-yl)methoxy)benzamide (A11)

White solid, Mp: 108–109 °C; ^1H NMR (600 MHz, Chloroform- d) δ 7.52 (s, 1H), 7.47 (d, $J = 7.7$ Hz, 1H), 7.30 (t, $J = 7.6$ Hz, 1H), 7.24 (d, $J = 7.6$ Hz, 1H), 7.10 (td, $J = 9.1$, 5.1 Hz, 1H), 6.88 (td, $J = 9.2$, 2.0 Hz, 1H), 5.92 (d, $J = 49.5$ Hz, 2H), 5.12–5.06 (m, 1H), 4.24–4.12 (m, 2H), 3.56–3.39 (m, 2H), 2.39 (s, 3H). ^{13}C NMR (150 MHz, DMSO- d_6) δ 161.76, 157.05, 152.51 (dd, $J_{F-C} = 241.3$, 6.6 Hz), 148.39 (dd, $J_{F-C} = 248.6$, 8.5 Hz), 143.38 (dd, $J_{F-C} = 10.9$, 3.2 Hz), 138.55, 131.24, 129.63, 129.18, 127.55, 124.28, 117.08 (dd, $J_{F-C} = 25.1$, 20.4 Hz), 116.31 (dd, $J_{F-C} = 9.4$, 2.4 Hz), 111.43 (dd, $J_{F-C} = 23.1$, 3.8 Hz), 78.99, 71.35, 37.07, 21.36. ESI-MS calcd for $\text{C}_{18}\text{H}_{17}\text{F}_2\text{N}_2\text{O}_3$ [M+H] $^+$, 347.3, found 347.3.

5.2.12. 2,6-Difluoro-3-((3-(*p*-tolyl)-4,5-dihydroisoxazol-5-yl)methoxy)benzamide (A12)

White solid, Mp: 135–137 °C; ^1H NMR (600 MHz, Chloroform- d) δ 7.58 (s, 2H), 7.22 (d, $J = 7.9$ Hz, 2H), 7.09 (td, $J = 9.0$, 5.3 Hz, 1H),

6.88 (td, $J = 9.1$, 2.0 Hz, 1H), 5.92 (d, $J = 45.6$ Hz, 2H), 5.08 (dq, $J = 11.1$, 5.1 Hz, 1H), 4.26 – 4.09 (m, 2H), 3.57–3.35 (m, 2H), 2.39 (s, 3H). ^{13}C NMR (150 MHz, DMSO- d_6) δ 161.75, 156.86, 152.50 (dd, $J_{F-C} = 241.6$, 6.6 Hz), 148.39 (dd, $J_{F-C} = 248.7$, 8.4 Hz), 143.38 (dd, $J_{F-C} = 11.0$, 3.2 Hz), 140.35, 129.85, 127.03, 126.92, 117.09 (dd, $J_{F-C} = 25.0$, 20.4 Hz), 116.29 (dd, $J_{F-C} = 9.2$, 2.4 Hz), 111.42 (dd, $J_{F-C} = 22.7$, 3.8 Hz), 78.89, 71.38, 37.12, 21.44. ESI-MS calcd for $\text{C}_{18}\text{H}_{17}\text{F}_2\text{N}_2\text{O}_3$ [M+H] $^+$, 347.3, found 347.3.

5.2.13. 2,6-Difluoro-3-((3-(4-ethylphenyl)-4,5-dihydroisoxazol-5-yl)methoxy)benzamide (A13)

White solid, Mp: 132–133 °C; ^1H NMR (600 MHz, Chloroform- d) δ 7.60 (d, $J = 8.2$ Hz, 2H), 7.24 (d, $J = 8.2$ Hz, 2H), 7.09 (td, $J = 9.1$, 5.1 Hz, 1H), 6.88 (td, $J = 9.1$, 2.0 Hz, 1H), 5.91 (d, $J = 47.4$ Hz, 2H), 5.11–5.04 (m, 1H), 4.25–4.10 (m, 2H), 3.57–3.36 (m, 2H), 2.68 (q, $J = 7.6$ Hz, 2H), 1.25 (t, $J = 7.6$ Hz, 3H). ^{13}C NMR (150 MHz, DMSO- d_6) δ 161.75, 156.88, 152.51 (dd, $J_{F-C} = 241.5$, 6.6 Hz), 148.39 (dd, $J_{F-C} = 248.6$, 8.5 Hz), 146.58, 143.38 (dd, $J_{F-C} = 10.7$, 3.2 Hz), 128.68, 127.14, 117.09 (dd, $J_{F-C} = 24.9$, 20.4 Hz), 116.30 (dd, $J_{F-C} = 9.3$, 2.3 Hz), 111.42 (dd, $J_{F-C} = 23.1$, 3.8 Hz), 78.89, 71.38, 37.14, 28.52, 15.85. ESI-MS calcd for $\text{C}_{19}\text{H}_{19}\text{F}_2\text{N}_2\text{O}_3$ [M+H] $^+$, 361.4, found 361.3.

5.2.14. 2,6-Difluoro-3-((3-(4-isopropylphenyl)-4,5-dihydroisoxazol-5-yl)methoxy)benzamide (A14)

White solid, Mp: 132–133 °C; ^1H NMR (600 MHz, Chloroform- d) δ 7.62 (d, $J = 8.2$ Hz, 2H), 7.28 (d, $J = 8.4$ Hz, 2H), 7.09 (td, $J = 9.1$, 5.1 Hz, 1H), 6.88 (td, $J = 9.1$, 2.0 Hz, 1H), 5.91 (d, $J = 49.5$ Hz, 2H), 5.12–5.04 (m, 1H), 4.24–4.10 (m, 2H), 3.55–3.38 (m, 2H), 2.98–2.90 (m, 1H), 1.26 (d, $J = 6.9$ Hz, 6H). ^{13}C NMR (150 MHz, DMSO- d_6) δ 161.75, 156.86, 152.51 (dd, $J_{F-C} = 241.5$, 6.6 Hz), 151.14, 148.39 (dd, $J_{F-C} = 248.6$, 8.6 Hz), 143.39 (dd, $J_{F-C} = 10.8$, 3.1 Hz), 127.32, 127.20 (d, $J_{F-C} = 6.7$ Hz), 117.09 (dd, $J_{F-C} = 24.9$, 20.4 Hz), 116.31 (dd, $J_{F-C} = 9.4$, 2.2 Hz), 111.43 (dd, $J_{F-C} = 22.8$, 3.8 Hz), 78.88, 71.37, 37.15, 33.82, 24.11. ESI-MS calcd for $\text{C}_{20}\text{H}_{21}\text{F}_2\text{N}_2\text{O}_3$ [M+H] $^+$, 375.4, found 375.4.

5.2.15. 2,6-Difluoro-3-((3-(4-*tert*-butylphenyl)-4,5-dihydroisoxazol-5-yl)methoxy)benzamide (A15)

White solid, Mp: 157–159 °C; ^1H NMR (600 MHz, Chloroform- d) δ 7.62 (d, $J = 8.4$ Hz, 2H), 7.44 (d, $J = 8.4$ Hz, 2H), 7.10 (td, $J = 9.1$, 5.0 Hz, 1H), 6.88 (td, $J = 9.1$, 2.0 Hz, 1H), 5.90 (d, $J = 59.7$ Hz, 2H), 5.08 (ddt, $J = 10.4$, 6.8, 5.0 Hz, 1H), 4.17 (ddd, $J = 47.7$, 10.3, 5.0 Hz, 2H), 3.56–3.37 (m, 2H), 1.34 (s, 9H). ^{13}C NMR (150 MHz, DMSO- d_6) δ 161.73, 156.79, 153.33, 153.28, 151.70 (d, $J_{F-C} = 6.6$ Hz), 148.39 (dd, $J_{F-C} = 248.5$, 8.5 Hz), 143.38 (dd, $J_{F-C} = 11.0$, 3.2 Hz), 126.95, 126.92, 126.07, 117.09 (dd, $J_{F-C} = 24.9$, 20.4 Hz), 116.36, 116.34, 116.29, 111.43 (dd, $J_{F-C} = 23.1$, 4.0 Hz), 78.87, 71.36, 37.14, 35.05, 31.39. ESI-MS calcd for $\text{C}_{21}\text{H}_{23}\text{F}_2\text{N}_2\text{O}_3$ [M+H] $^+$, 389.4, found 389.3.

5.2.16. 2,6-Difluoro-3-((3-(4-butylphenyl)-4,5-dihydroisoxazol-5-yl)methoxy)benzamide (A16)

White solid, Mp: 143–144 °C; ^1H NMR (600 MHz, Chloroform- d) δ 7.59 (d, $J = 8.1$ Hz, 2H), 7.23 (d, $J = 8.1$ Hz, 2H), 7.09 (td, $J = 9.1$, 5.1 Hz, 1H), 6.88 (td, $J = 9.1$, 2.0 Hz, 1H), 5.93 (d, $J = 34.7$ Hz, 2H), 5.11 – 5.05 (m, 1H), 4.24–4.10 (m, 2H), 3.55–3.37 (m, 2H), 2.64 (t, 2H), 1.64–1.58 (m, 2H), 1.36 (h, $J = 7.4$ Hz, 2H), 0.93 (t, $J = 7.3$ Hz, 3H). ^{13}C NMR (150 MHz, DMSO- d_6) δ 161.72, 156.88, 152.53 (dd, $J_{F-C} = 242.4$, 7.1 Hz), 148.42 (dd, $J_{F-C} = 249.5$, 9.1 Hz), 145.17, 143.42 (dd, $J_{F-C} = 11.1$, 3.5 Hz), 129.19, 127.17, 127.07, 128.61, 117.12 (dd, $J_{F-C} = 25.3$, 20.2 Hz), 116.43 (d, $J_{F-C} = 10.1$ Hz), 111.42 (dd, $J_{F-C} = 22.2$, 4.5 Hz), 78.89, 71.40, 37.15, 35.11, 33.35, 22.15, 14.21. ESI-MS calcd for $\text{C}_{21}\text{H}_{23}\text{F}_2\text{N}_2\text{O}_3$ [M+H] $^+$, 389.4, found 389.3.

5.2.17. 2,6-Difluoro-3-((3-(4-pentylphenyl)-4,5-dihydroisoxazol-5-yl)methoxy)benzamide (A17)

White solid, Mp: 148–149 °C; ^1H NMR (600 MHz, DMSO- d_6) δ 8.12

(s, 1H), 7.83 (s, 1H), 7.59 (d, $J = 8.2$ Hz, 2H), 7.28 (d, $J = 8.3$ Hz, 2H), 7.27–7.23 (m, 1H), 7.07 (td, $J = 9.0$, 1.8 Hz, 1H), 5.08–5.02 (m, 1H), 4.24–4.15 (m, 2H), 3.58 (dd, $J = 17.0$, 11.0 Hz, 1H), 3.29 (dd, $J = 17.0$, 7.2 Hz, 1H), 2.61 (t, $J = 7.6$ Hz, 2H), 1.58 (p, $J = 7.6$ Hz, 2H), 1.34–1.23 (m, 4H), 0.86 (t, $J = 7.1$ Hz, 3H). ^{13}C NMR (150 MHz, DMSO- d_6) δ 161.73, 156.89, 152.50 (dd, $J_{F-C} = 241.5$, 6.7 Hz), 148.39 (dd, $J_{F-C} = 248.8$, 8.4 Hz), 145.19, 143.38 (dd, $J_{F-C} = 10.9$, 3.2 Hz), 129.20, 127.17, 127.07, 117.09 (dd, $J_{F-C} = 25.0$, 20.4 Hz), 116.35, 116.33, 116.28, 111.42 (dd, $J_{F-C} = 22.8$, 3.8 Hz), 78.88, 71.36, 37.14, 35.39, 31.28, 30.88, 22.40, 14.38. ESI-MS calcd for $\text{C}_{22}\text{H}_{25}\text{F}_2\text{N}_2\text{O}_3$ $[\text{M} + \text{H}]^+$, 403.4, found 403.5.

5.2.18. 2,6-Difluoro-3-((3-(4-cyclohexylphenyl)-4,5-dihydroisoxazol-5-yl)methoxy)benzamide (A18)

White solid, Mp: 178–180 °C; ^1H NMR (600 MHz, DMSO- d_6) δ 8.11 (s, 1H), 7.83 (s, 1H), 7.60 (d, $J = 8.3$ Hz, 2H), 7.31 (d, $J = 8.3$ Hz, 2H), 7.25 (td, $J = 9.3$, 5.2 Hz, 1H), 7.07 (td, $J = 9.0$, 1.8 Hz, 1H), 5.09–5.01 (m, 1H), 4.23–4.15 (m, 2H), 3.57 (dd, $J = 17.0$, 11.0 Hz, 1H), 3.28 (dd, $J = 17.1$, 7.2 Hz, 1H), 2.58–2.52 (m, 1H), 1.82–1.76 (m, 4H), 1.71 (d, $J = 12.7$ Hz, 1H), 1.45–1.33 (m, 4H), 1.28–1.20 (m, 1H). ^{13}C NMR (150 MHz, DMSO- d_6) δ 161.73, 156.87, 152.51 (dd, $J_{F-C} = 241.2$, 6.7 Hz), 150.28, 148.40 (dd, $J_{F-C} = 248.8$, 8.3 Hz), 143.38 (dd, $J_{F-C} = 10.9$, 3.2 Hz), 127.58, 127.33, 127.15, 117.09 (dd, $J_{F-C} = 25.0$, 20.4 Hz), 116.32 (dd, $J_{F-C} = 9.3$, 2.3 Hz), 111.42 (dd, $J_{F-C} = 22.8$, 3.8 Hz), 78.86, 71.36, 44.11, 37.14, 34.19, 26.73, 26.00. ESI-MS calcd for $\text{C}_{23}\text{H}_{25}\text{F}_2\text{N}_2\text{O}_3$ $[\text{M} + \text{H}]^+$, 415.5, found 415.4.

5.2.19. 2,6-Difluoro-3-((3-(2-methoxyphenyl)-4,5-dihydroisoxazol-5-yl)methoxy)benzamide (A19)

White solid, Mp: 108–109 °C; ^1H NMR (600 MHz, Chloroform- d) δ 7.74–7.70 (m, 1H), 7.42–7.37 (m, 1H), 7.10 (td, $J = 9.1$, 5.1 Hz, 1H), 6.98 (t, $J = 7.5$ Hz, 1H), 6.95 (d, $J = 8.4$ Hz, 1H), 6.88 (td, $J = 9.1$, 2.0 Hz, 1H), 5.93 (d, $J = 55.4$ Hz, 2H), 5.07–5.01 (m, 1H), 4.22–4.10 (m, 2H), 3.87 (s, 3H), 3.69–3.45 (m, 2H). ^{13}C NMR (150 MHz, DMSO- d_6) δ 161.78, 157.75, 156.11, 152.48 (dd, $J_{F-C} = 241.3$, 6.6 Hz), 148.37 (dd, $J_{F-C} = 248.7$, 8.4 Hz), 143.42 (dd, $J_{F-C} = 11.0$, 3.2 Hz), 131.98, 129.37, 121.07, 118.66, 117.09 (dd, $J_{F-C} = 25.0$, 20.4 Hz), 116.22 (dd, $J_{F-C} = 9.4$, 2.3 Hz), 112.68, 111.41 (dd, $J_{F-C} = 22.8$, 3.9 Hz), 78.79, 71.33, 56.16, 26.81. ESI-MS calcd for $\text{C}_{18}\text{H}_{17}\text{F}_2\text{N}_2\text{O}_4$ $[\text{M} + \text{H}]^+$, 363.3, found 363.3.

5.2.20. 2,6-Difluoro-3-((3-(3-methoxyphenyl)-4,5-dihydroisoxazol-5-yl)methoxy)benzamide (A20)

White solid, Mp: 114–116 °C; ^1H NMR (600 MHz, DMSO- d_6) δ 8.11 (s, 1H), 7.83 (s, 1H), 7.38 (t, $J = 8.0$ Hz, 1H), 7.30–7.20 (m, 3H), 7.11–7.02 (m, 2H), 5.12–5.04 (m, 1H), 4.26–4.15 (m, 2H), 3.80 (s, 3H), 3.59 (dd, $J = 17.1$, 11.0 Hz, 1H), 3.30–3.27 (m, 1H). ^{13}C NMR (150 MHz, DMSO- d_6) δ 161.72, 159.81, 157.00, 152.50 (dd, $J_{F-C} = 241.6$, 6.7 Hz), 148.38 (dd, $J_{F-C} = 248.6$, 8.5 Hz), 143.37 (dd, $J_{F-C} = 10.9$, 3.2 Hz), 131.00, 130.45, 119.60, 117.09 (dd, $J_{F-C} = 24.9$, 20.5 Hz), 116.47, 116.33 (d, $J_{F-C} = 8.4$ Hz), 112.02, 111.44 (dd, $J_{F-C} = 23.0$, 4.1 Hz), 79.16, 71.35, 55.69, 37.09. ESI-MS calcd for $\text{C}_{18}\text{H}_{17}\text{F}_2\text{N}_2\text{O}_4$ $[\text{M} + \text{H}]^+$, 363.3, found 363.3.

5.2.21. 2,6-Difluoro-3-((3-(4-methoxyphenyl)-4,5-dihydroisoxazol-5-yl)methoxy)benzamide (A21)

White solid, Mp: 175–176 °C; ^1H NMR (600 MHz, Chloroform- d) δ 7.63 (d, $J = 8.5$ Hz, 2H), 7.14–7.05 (m, 1H), 6.98–6.84 (m, 3H), 5.93 (d, $J = 50.0$ Hz, 2H), 5.11–5.02 (m, 1H), 4.25–4.08 (m, 2H), 3.85 (s, 3H), 3.55–3.34 (m, 2H). ^{13}C NMR (150 MHz, DMSO- d_6) δ 161.74, 161.13, 156.49, 152.49 (dd, $J_{F-C} = 241.5$, 6.7 Hz), 148.38 (dd, $J_{F-C} = 248.8$, 8.4 Hz), 143.39 (dd, $J_{F-C} = 10.8$, 3.1 Hz), 128.68, 122.13, 117.08 (dd, $J_{F-C} = 24.9$, 20.4 Hz), 116.29 (dd, $J_{F-C} = 9.5$, 2.3 Hz), 114.71, 111.42 (dd, $J_{F-C} = 23.1$, 3.8 Hz), 78.73, 71.38, 55.76, 37.31. ESI-MS calcd for $\text{C}_{18}\text{H}_{17}\text{F}_2\text{N}_2\text{O}_4$ $[\text{M} + \text{H}]^+$, 363.3, found 363.3.

5.2.22. 2,6-Difluoro-3-((3-(3-ethoxyphenyl)-4,5-dihydroisoxazol-5-yl)methoxy)benzamide (A22)

White solid, Mp: 152–153 °C; ^1H NMR (400 MHz, DMSO- d_6) δ 8.11 (s, 1H), 7.83 (s, 1H), 7.41–7.33 (m, 1H), 7.30–7.16 (m, 3H), 7.12–6.99 (m, 2H), 5.13–5.02 (m, 1H), 4.28–4.13 (m, 2H), 4.06 (q, $J = 7.0$ Hz, 2H), 3.59 (dd, $J = 17.1$, 11.0 Hz, 1H), 3.3–3.23 (m, 1H), 1.34 (t, $J = 7.0$ Hz, 3H). ^{13}C NMR (150 MHz, DMSO- d_6) δ 161.72, 159.08, 157.01, 151.72, 147.53, 143.41, 130.98, 130.44, 119.45, 117.09 (dd, $J_{F-C} = 25.1$, 20.1 Hz), 116.85, 116.33 (d, $J_{F-C} = 8.2$ Hz), 112.59, 111.44 (dd, $J_{F-C} = 23.1$, 3.6 Hz), 79.13, 71.35, 63.64, 37.08, 15.06. ESI-MS calcd for $\text{C}_{19}\text{H}_{19}\text{F}_2\text{N}_2\text{O}_4$ $[\text{M} + \text{H}]^+$, 377.4, found 377.5.

5.2.23. 2,6-Difluoro-3-((3-(4-ethoxyphenyl)-4,5-dihydroisoxazol-5-yl)methoxy)benzamide (A23)

White solid, Mp: 132–134 °C; ^1H NMR (600 MHz, DMSO- d_6) δ 8.11 (s, 1H), 7.83 (s, 1H), 7.61 (d, $J = 8.9$ Hz, 2H), 7.25 (td, $J = 9.3$, 5.2 Hz, 1H), 7.07 (td, $J = 8.9$, 1.8 Hz, 1H), 6.99 (d, $J = 8.9$ Hz, 2H), 5.03 (dd, $J = 10.8$, 6.0 Hz, 1H), 4.23–4.14 (m, 2H), 4.07 (q, $J = 7.0$ Hz, 2H), 3.56 (dd, $J = 17.0$, 10.9 Hz, 1H), 3.27 (dd, $J = 17.0$, 7.3 Hz, 1H), 1.34 (t, $J = 7.0$ Hz, 3H). ^{13}C NMR (150 MHz, DMSO- d_6) δ 161.74, 160.42, 156.49, 152.49 (dd, $J_{F-C} = 241.5$, 6.6 Hz), 148.38 (dd, $J_{F-C} = 248.7$, 8.4 Hz), 143.39 (dd, $J_{F-C} = 11.0$, 3.2 Hz), 128.68, 121.97, 117.09 (dd, $J_{F-C} = 25.0$, 20.4 Hz), 116.34, 116.33, 116.27, 115.11, 111.42 (dd, $J_{F-C} = 22.8$, 3.8 Hz), 78.71, 71.38, 63.72, 37.30, 15.01. ESI-MS calcd for $\text{C}_{19}\text{H}_{19}\text{F}_2\text{N}_2\text{O}_4$ $[\text{M} + \text{H}]^+$, 377.4, found 377.5.

5.2.24. 2,6-Difluoro-3-((3-(3-propoxyphenyl)-4,5-dihydroisoxazol-5-yl)methoxy)benzamide (A24)

White solid, Mp: 145–146 °C; ^1H NMR (600 MHz, Chloroform- d) δ 7.31 (t, $J = 8.0$ Hz, 1H), 7.27 (d, $J = 2.3$ Hz, 1H), 7.20 (d, $J = 7.7$ Hz, 1H), 7.10 (td, $J = 9.1$, 5.1 Hz, 1H), 6.99–6.94 (m, 1H), 6.88 (td, $J = 9.1$, 2.0 Hz, 1H), 5.92 (d, $J = 46.0$ Hz, 2H), 5.13–5.06 (m, 1H), 4.24–4.12 (m, 2H), 3.95 (t, $J = 6.6$ Hz, 2H), 3.55–3.38 (m, 2H), 1.82 (h, $J = 7.3$ Hz, 2H), 1.04 (t, $J = 7.4$ Hz, 3H). ^{13}C NMR (150 MHz, DMSO- d_6) δ 161.73, 159.25, 157.02, 152.51 (dd, $J_{F-C} = 241.5$, 6.6 Hz), 148.39 (dd, $J_{F-C} = 248.7$, 8.4 Hz), 143.37 (dd, $J_{F-C} = 10.9$, 3.2 Hz), 130.98, 130.43, 119.44, 117.09 (dd, $J_{F-C} = 25.0$, 20.3 Hz), 116.87, 116.33 (d, $J_{F-C} = 9.3$ Hz), 112.65, 111.43 (dd, $J_{F-C} = 23.0$, 3.9 Hz), 79.14, 71.36, 69.53, 37.08, 22.47, 10.85. ESI-MS calcd for $\text{C}_{20}\text{H}_{21}\text{F}_2\text{N}_2\text{O}_4$ $[\text{M} + \text{H}]^+$, 391.4, found 391.3.

5.2.25. 2,6-Difluoro-3-((3-(4-propoxyphenyl)-4,5-dihydroisoxazol-5-yl)methoxy)benzamide (A25)

White solid, Mp: 162–163 °C; ^1H NMR (600 MHz, Chloroform- d) δ 7.61 (d, $J = 8.9$ Hz, 2H), 7.10 (td, $J = 9.1$, 5.1 Hz, 1H), 6.92 (d, $J = 8.9$ Hz, 2H), 6.88 (td, $J = 9.1$, 1.9 Hz, 1H), 5.91 (d, $J = 61.0$ Hz, 2H), 5.06 (ddt, $J = 10.5$, 6.9, 5.1 Hz, 1H), 4.17 (ddd, $J = 48.3$, 10.2, 5.1 Hz, 2H), 3.96 (t, $J = 6.5$ Hz, 2H), 3.54–3.35 (m, 2H), 1.87–1.79 (m, 2H), 1.05 (t, $J = 7.4$ Hz, 3H). ^{13}C NMR (150 MHz, DMSO- d_6) δ 161.73, 160.57, 156.48, 152.48 (dd, $J_{F-C} = 241.6$, 6.6 Hz), 148.37 (dd, $J_{F-C} = 248.7$, 8.4 Hz), 143.38 (dd, $J_{F-C} = 10.8$, 3.1 Hz), 128.66, 121.97, 117.08 (dd, $J_{F-C} = 24.9$, 20.4 Hz), 116.33, 115.15, 111.41 (dd, $J_{F-C} = 22.8$, 3.8 Hz), 78.70, 71.38, 69.56, 37.30, 22.42, 10.81. ESI-MS calcd for $\text{C}_{20}\text{H}_{21}\text{F}_2\text{N}_2\text{O}_4$ $[\text{M} + \text{H}]^+$, 391.4, found 391.3.

5.2.26. 2,6-Difluoro-3-((3-(benzo[d][1,3]dioxol-5-yl)-4,5-dihydroisoxazol-5-yl)methoxy)benzamide (A26)

White solid, Mp: 150–152 °C; ^1H NMR (600 MHz, Chloroform- d) δ 7.29 (d, $J = 1.6$ Hz, 1H), 7.12–7.04 (m, 2H), 6.89 (td, $J = 9.1$, 2.0 Hz, 1H), 6.83 (d, $J = 8.1$ Hz, 1H), 6.01 (s, 2H), 5.91 (d, $J = 59.7$ Hz, 2H), 5.10–5.03 (m, 1H), 4.24–4.10 (m, 2H), 3.52–3.33 (m, 2H). ^{13}C NMR (150 MHz, DMSO- d_6) δ 161.75, 156.61, 152.50 (dd, $J_{F-C} = 241.5$, 6.6 Hz), 149.37, 148.19, 147.56 (d, $J_{F-C} = 8.5$ Hz), 143.37 (dd, $J_{F-C} = 11.0$, 3.2 Hz), 123.68, 122.12, 117.08 (dd, $J_{F-C} = 24.9$, 20.4 Hz), 116.31 (dd, $J_{F-C} = 9.4$, 2.2 Hz), 111.42 (dd, $J_{F-C} = 23.1$, 3.8 Hz), 108.89, 106.44, 102.03, 78.96, 71.35, 37.29. ESI-MS calcd for

$C_{18}H_{15}F_2N_2O_5$ [M+H]⁺, 377.3, found 377.3.

5.2.27. 2,6-Difluoro-3-((3-(furan-2-yl)-4,5-dihydroisoxazol-5-yl) methoxy)benzamide (A27)

White solid, Mp: 168–169 °C; ¹H NMR (600 MHz, Chloroform-*d*) δ 7.53 (d, *J* = 1.8 Hz, 1H), 7.09 (td, *J* = 9.1, 5.1 Hz, 1H), 6.89 (td, *J* = 9.2, 2.0 Hz, 1H), 6.76 (d, *J* = 3.5 Hz, 1H), 6.51 (dd, *J* = 3.5, 1.8 Hz, 1H), 5.93 (d, *J* = 53.6 Hz, 2H), 5.10–5.02 (m, 1H), 4.24–4.10 (m, 2H), 3.54–3.36 (m, 2H). ESI-MS calcd for $C_{15}H_{13}F_2N_2O_4$ [M+H]⁺, 323.3, found 323.3.

5.3. Typical compounds of the series B

5.3.1. 2,6-Difluoro-3-((5-(2-chlorophenyl)-4,5-dihydroisoxazol-3-yl) methoxy)benzamide (B1)

White solid, Mp: 106–109 °C; ¹H NMR (600 MHz, Chloroform-*d*) δ 7.43–7.41 (dd, *J* = 6.9, 2.5 Hz, 1H), 7.39–7.37 (m, 1H), 7.28–7.27 (m, 1H), 7.26–7.24 (m, 1H), 7.11–7.07 (td, *J* = 9.1, 5.0 Hz, 1H), 6.89–6.86 (td, *J* = 9.1, 2.0 Hz, 1H), 5.96–5.85 (m, 3H), 4.93–4.87 (m, 2H), 3.73–3.68 (dd, *J* = 17.6, 11.3 Hz, 1H), 3.00–2.96 (dd, *J* = 17.6, 7.2 Hz, 1H). ESI-MS calcd for $C_{17}H_{13}ClF_2N_2O_3$ [M+H]⁺, 367.1, [M+NH₄]⁺, 384.1, found 367.2, 384.2.

5.3.2. 2,6-Difluoro-3-((5-(3-chlorophenyl)-4,5-dihydroisoxazol-3-yl) methoxy)benzamide (B2)

Waxy solid, Mp: 108–112 °C; ¹H NMR (600 MHz, Chloroform-*d*) δ 7.30–7.27 (m, 3H), 7.17–7.09 (m, 2H), 6.92–6.88 (td, *J* = 9.1, 1.9 Hz, 1H), 5.97–5.94 (d, *J* = 13.8 Hz, 2H), 5.65–5.62 (dd, *J* = 11.1, 7.8 Hz, 1H), 4.93 (s, 2H), 3.59–3.55 (dd, *J* = 17.4, 11.2 Hz, 1H), 3.08–3.04 (dd, *J* = 17.4, 7.8 Hz, 1H). ¹³C NMR (150 MHz, DMSO-*d*₆) δ 161.65, 155.67, 152.87 (dd, *J*_{F-C} = 242.1, 6.7 Hz), 148.63 (dd, *J*_{F-C} = 249.0, 8.4 Hz), 143.92, 142.59 (dd, *J*_{F-C} = 11.0, 3.2 Hz), 133.77, 131.06, 128.50, 126.31, 125.12, 117.19 (dd, *J*_{F-C} = 25.0, 20.4 Hz), 116.92 (d, *J*_{F-C} = 9.3 Hz), 111.50 (dd, *J*_{F-C} = 23.1, 3.8 Hz), 81.07, 64.66, 42.99. ESI-MS calcd for $C_{17}H_{13}ClF_2N_2O_3$ [M+H]⁺, 367.1, [M+NH₄]⁺, 384.1, found 367.2, 384.3.

5.3.3. 2,6-Difluoro-3-((5-(4-chlorophenyl)-4,5-dihydroisoxazol-3-yl) methoxy)benzamide (B3)

White solid, Mp: 127–129 °C; ¹H NMR (600 MHz, DMSO-*d*₆) δ 8.14 (s, 1H), 7.87 (s, 1H), 7.45 (d, *J* = 8.5 Hz, 2H), 7.35–7.29 (m, 3H), 7.10 (td, *J* = 8.9, 1.7 Hz, 1H), 5.67 (dd, *J* = 11.1, 8.0 Hz, 1H), 5.01 (s, 2H), 3.58 (dd, *J* = 17.5, 11.1 Hz, 1H), 3.03 (dd, *J* = 17.6, 8.0 Hz, 1H). ¹³C NMR (150 MHz, DMSO-*d*₆) δ 160.55, 154.51, 151.74 (dd, *J*_{F-C} = 244.6, 6.8 Hz), 147.48 (dd, *J*_{F-C} = 249.2, 9.1 Hz), 141.44 (dd, *J*_{F-C} = 12.1, 4.5 Hz), 139.30, 132.04, 128.01, 127.32, 116.19 (d, *J*_{F-C} = 19.6 Hz), 115.90 (d, *J*_{F-C} = 16.6 Hz), 110.51 (dd, *J*_{F-C} = 22.7, 6.8 Hz), 80.09, 63.59, 41.85. ESI-MS calcd for $C_{17}H_{14}ClF_2N_2O_3$ [M+H]⁺, 367.1, found 367.2.

5.3.4. 2,6-Difluoro-3-((5-(2,4-dichlorophenyl)-4,5-dihydroisoxazol-3-yl) methoxy)benzamide (B4)

White solid, Mp: 108–112 °C; ¹H NMR (600 MHz, Chloroform-*d*) δ 7.41–7.40 (d, *J* = 2.0 Hz, 1H), 7.37–7.36 (dd, *J* = 8.4, 0.7 Hz, 1H), 7.26–7.25 (m, 1H), 7.11–7.07 (td, *J* = 9.1, 5.1 Hz, 1H), 6.90–6.87 (td, *J* = 9.1, 2.1 Hz, 1H), 5.95–5.87 (m, 3H), 4.92–4.86 (m, 2H), 3.73–3.68 (dd, *J* = 17.6, 11.3 Hz, 1H), 2.97–2.93 (dd, *J* = 17.6, 7.1 Hz, 1H). ¹³C NMR (150 MHz, DMSO-*d*₆) δ 161.62, 155.74, 152.89 (dd, *J*_{F-C} = 242.2, 6.6 Hz), 148.64 (dd, *J*_{F-C} = 248.9, 8.4 Hz), 142.53 (dd, *J*_{F-C} = 11.0, 3.3 Hz), 137.92, 133.82, 132.25, 129.62, 128.71, 128.17, 117.31, 117.03 (dd, *J*_{F-C} = 8.4, 2.6 Hz), 111.49 (dd, *J*_{F-C} = 23.3, 3.7 Hz), 78.64, 64.58, 42.46. ESI-MS calcd for $C_{17}H_{12}Cl_2F_2N_2O_3$ [M+H]⁺, 401.1, [M+NH₄]⁺, 418.1, found 401.2, 418.3.

5.3.5. 2,6-Difluoro-3-((5-(3,4-dichlorophenyl)-4,5-dihydroisoxazol-3-yl) methoxy)benzamide (B5)

White solid, Mp: 114–119 °C; ¹H NMR (600 MHz, Chloroform-*d*) δ 7.44–7.43 (d, *J* = 8.3 Hz, 1H), 7.38 (d, *J* = 2.1 Hz, 1H), 7.13–7.09 (m, 2H), 6.92–6.89 (td, *J* = 9.1, 2.0 Hz, 1H), 5.97–5.93 (d, *J* = 22.8 Hz, 2H), 5.64–5.60 (dd, *J* = 11.1, 7.6 Hz, 1H), 4.92 (s, 2H), 3.60–3.55 (dd, *J* = 17.4, 11.1 Hz, 1H), 3.06–3.02 (dd, *J* = 17.4, 7.6 Hz, 1H). ¹³C NMR (150 MHz, DMSO-*d*₆) δ 161.63, 155.76, 152.88 (dd, *J*_{F-C} = 242.2, 6.6 Hz), 148.64 (dd, *J*_{F-C} = 249.0, 8.5 Hz), 142.59 (d, *J*_{F-C} = 3.3 Hz), 142.53, 131.75, 131.36, 131.12, 128.53, 126.75, 117.19 (dd, *J*_{F-C} = 25.0, 20.4 Hz), 116.97 (d, *J*_{F-C} = 9.4 Hz), 111.50 (dd, *J*_{F-C} = 22.9, 3.9 Hz), 80.44, 64.64, 42.98. ESI-MS calcd for $C_{17}H_{12}Cl_2F_2N_2O_3$ [M+H]⁺, 401.1, [M+NH₄]⁺, 418.1, found 401.2, 418.3.

5.3.6. 2,6-Difluoro-3-((5-(4-fluorophenyl)-4,5-dihydroisoxazol-3-yl) methoxy)benzamide (B6)

Waxy solid, Mp: 99–103 °C; ¹H NMR (600 MHz, Chloroform-*d*) δ 7.28–7.27 (m, 1H), 7.26 (s, 1H), 7.14–7.10 (td, *J* = 9.1, 5.1 Hz, 1H), 7.06–7.03 (t, *J* = 8.7 Hz, 2H), 6.92–6.88 (td, *J* = 9.1, 2.0 Hz, 1H), 5.96 (s, 2H), 5.66–5.63 (dd, *J* = 11.0, 8.3 Hz, 1H), 4.95–4.90 (d, *J* = 2.9 Hz, 2H), 3.57–3.52 (dd, *J* = 17.4, 11.1 Hz, 1H), 3.09–3.04 (dd, *J* = 17.4, 8.3 Hz, 1H). ¹³C NMR (150 MHz, DMSO-*d*₆) δ 163.15, 161.69, 161.53, 155.58, 152.90 (dd, *J*_{F-C} = 242.2, 6.6 Hz), 148.70 (dd, *J*_{F-C} = 248.9, 8.4 Hz), 142.60 (dd, *J*_{F-C} = 10.7, 3.3 Hz), 137.52 (d, *J*_{F-C} = 3.1 Hz), 128.69 (d, *J*_{F-C} = 8.3 Hz), 117.20 (d, *J*_{F-C} = 4.6 Hz), 117.07 (d, *J*_{F-C} = 7.6 Hz), 115.90 (d, *J*_{F-C} = 21.5 Hz), 111.53 (dd, *J*_{F-C} = 23.2, 3.9 Hz), 81.38, 64.77, 42.87. ESI-MS calcd for $C_{17}H_{13}F_3N_2O_3$ [M+H]⁺, 351.1, [M+NH₄]⁺, 368.1, found 351.3, 368.3.

5.3.7. 2,6-Difluoro-3-((5-(4-bromophenyl)-4,5-dihydroisoxazol-3-yl) methoxy)benzamide (B7)

White solid, Mp: 122–124 °C; ¹H NMR (600 MHz, Chloroform-*d*) δ 7.50–7.48 (d, *J* = 8.4 Hz, 2H), 7.17–7.16 (d, *J* = 8.4 Hz, 2H), 7.13–7.09 (td, *J* = 9.1, 5.1 Hz, 1H), 6.91–6.88 (td, *J* = 9.1, 2.0 Hz, 1H), 5.95 (s, 2H), 5.64–5.61 (dd, *J* = 11.1, 8.1 Hz, 1H), 4.94–4.89 (m, 2H), 3.58–3.53 (dd, *J* = 17.4, 11.1 Hz, 1H), 3.07–3.02 (dd, *J* = 17.4, 8.0 Hz, 1H). ¹³C NMR (150 MHz, DMSO-*d*₆) δ 161.65, 155.59, 152.87 (dd, *J*_{F-C} = 242.2, 6.7 Hz), 148.65 (dd, *J*_{F-C} = 249.0, 8.5 Hz), 142.56 (dd, *J*_{F-C} = 10.7, 3.2 Hz), 140.80, 132.01, 128.70, 121.69, 117.18 (d, *J*_{F-C} = 4.5 Hz), 117.06 (d, *J*_{F-C} = 8.6 Hz), 111.53 (dd, *J*_{F-C} = 23.2, 3.8 Hz), 81.23, 64.71, 42.90. ESI-MS calcd for $C_{17}H_{13}BrF_2N_2O_3$ [M+H]⁺, 411.1, [M+NH₄]⁺, 428.1, found 411.2, 430.3.

5.3.8. 2,6-Difluoro-3-((5-(3-methylphenyl)-4,5-dihydroisoxazol-3-yl) methoxy)benzamide (B8)

Waxy solid, Mp: 78–80 °C; ¹H NMR (600 MHz, Chloroform-*d*) δ 7.26–7.23 (t, *J* = 7.6 Hz, 1H), 7.15–7.06 (m, 4H), 6.91–6.88 (td, *J* = 9.1, 2.1 Hz, 1H), 5.97 (s, 2H), 5.64–5.61 (dd, *J* = 11.1, 8.3 Hz, 1H), 4.95–4.90 (m, 2H), 3.55–3.51 (dd, *J* = 17.4, 11.1 Hz, 1H), 3.11–3.06 (dd, *J* = 17.4, 8.3 Hz, 1H), 2.34 (s, 3H). ¹³C NMR (150 MHz, DMSO-*d*₆) δ 161.65, 155.45, 152.85 (dd, *J*_{F-C} = 242.1, 6.6 Hz), 148.64 (dd, *J*_{F-C} = 248.9, 8.5 Hz), 142.61 (dd, *J*_{F-C} = 11.0, 3.2 Hz), 141.29, 138.32, 129.21, 128.98, 127.00, 123.65, 117.20 (dd, *J*_{F-C} = 24.9, 20.4 Hz), 116.92 (dd, *J*_{F-C} = 9.4, 2.2 Hz), 111.51 (dd, *J*_{F-C} = 23.2, 3.8 Hz), 82.07, 64.72, 42.86, 21.45. ESI-MS calcd for $C_{18}H_{16}F_2N_2O_3$ [M+H]⁺, 347.1, [M+NH₄]⁺, 364.1, found 347.3, 364.3.

5.3.9. 2,6-Difluoro-3-((5-(4-methylphenyl)-4,5-dihydroisoxazol-3-yl) methoxy)benzamide (B9)

White solid, Mp: 106–110 °C; ¹H NMR (600 MHz, Chloroform-*d*) δ 7.26 (s, 1H), 7.18–7.11 (m, 4H), 6.91–6.88 (td, *J* = 9.1, 2.1 Hz, 1H), 5.95 (s, 2H), 5.64–5.61 (dd, *J* = 11.1, 8.4 Hz, 1H), 4.95–4.90 (m, 2H), 3.54–3.49 (dd, *J* = 17.4, 11.1 Hz, 1H), 3.10–3.05 (dd, *J* = 17.4, 8.4 Hz, 1H), 2.35 (s, 3H). ¹³C NMR (150 MHz, DMSO-*d*₆) δ 161.65, 155.46, 152.85 (dd, *J*_{F-C} = 241.9, 6.6 Hz), 148.65 (dd, *J*_{F-C} = 248.8, 8.4 Hz), 142.62 (dd, *J*_{F-C} = 10.8, 3.3 Hz), 138.28, 137.91, 129.61, 126.53,

117.20 (d, $J_{F-C} = 4.7$ Hz), 116.98 (dd, $J_{F-C} = 9.7, 2.2$ Hz), 111.51 (dd, $J_{F-C} = 23.2, 3.8$ Hz), 82.02, 64.79, 42.74, 21.18. ESI-MS calcd for $C_{18}H_{16}F_2N_2O_3$ $[M+H]^+$, 347.1, $[M+NH_4]^+$, 364.1, found 347.3, 364.3.

5.3.10. 2,6-Difluoro-3-((5-(4-ethylphenyl)-4,5-dihydroisoxazol-3-yl)methoxy)benzamide (B10)

Waxy solid, Mp: 86–88 °C; 1H NMR (600 MHz, Chloroform-*d*) δ 7.21–7.18 (m, 4H), 7.15–7.11 (td, $J = 9.1, 5.1$ Hz, 1H), 6.91–6.88 (td, $J = 9.1, 2.0$ Hz, 1H), 5.95–5.92 (d, $J = 18.1$ Hz, 2H), 5.65–5.62 (dd, $J = 11.1, 8.5$ Hz, 1H), 4.95–4.90 (m, 2H), 3.54–3.49 (dd, $J = 17.4, 11.1$ Hz, 1H), 3.11–3.07 (dd, $J = 17.4, 8.5$ Hz, 1H), 2.6–2.63 (q, $J = 7.6$ Hz, 2H), 1.24–1.22 (t, $J = 7.6$ Hz, 3H). ^{13}C NMR (150 MHz, DMSO-*d*₆) δ 161.66, 155.46, 152.86 (dd, $J_{F-C} = 242.2, 6.7$ Hz), 148.66 (dd, $J_{F-C} = 248.8, 8.3$ Hz), 144.26, 142.62 (dd, $J_{F-C} = 11.0, 3.3$ Hz), 138.52, 128.45, 126.60, 117.19 (d, $J_{F-C} = 4.7$ Hz), 116.98 (d, $J_{F-C} = 9.3$ Hz), 111.51 (dd, $J_{F-C} = 23.2, 3.8$ Hz), 82.04, 64.78, 42.72, 28.33, 16.04. ESI-MS calcd for $C_{19}H_{18}F_2N_2O_3$ $[M+H]^+$, 361.1, $[M+NH_4]^+$, 378.1, found 361.3, 378.4.

5.3.11. 2,6-Difluoro-3-((5-(4-isopropylphenyl)-4,5-dihydroisoxazol-3-yl)methoxy)benzamide (B11)

White solid, Mp: 88–90 °C; 1H NMR (600 MHz, Chloroform-*d*) δ 7.26 (s, 1H), 7.24–7.22 (m, 1H), 7.21–7.17 (m, 2H), 7.15–7.11 (td, $J = 9.1, 5.1$ Hz, 1H), 6.91–6.88 (td, $J = 9.1, 2.0$ Hz, 1H), 5.97–5.93 (d, $J = 22.8$ Hz, 2H), 5.65–5.61 (dd, $J = 11.1, 8.5$ Hz, 1H), 4.959–4.90 (m, 2H), 3.54–3.49 (dd, $J = 17.4, 11.1$ Hz, 1H), 3.12–3.08 (dd, $J = 17.4, 8.5$ Hz, 1H), 2.93–2.87 (h, $J = 6.9$ Hz, 1H), 1.25–1.24 (d, $J = 6.9$ Hz, 6H). ^{13}C NMR (150 MHz, DMSO-*d*₆) δ 161.69, 155.46, 152.89 (dd, $J_{F-C} = 242.2, 6.6$ Hz), 149.53 (d, $J_{F-C} = 8.4$ Hz), 148.89, 147.87 (d, $J_{F-C} = 8.5$ Hz), 142.64 (dd, $J_{F-C} = 11.0, 3.3$ Hz), 138.63, 126.99, 126.62, 117.21 (d, $J_{F-C} = 4.6$ Hz), 116.99 (d, $J_{F-C} = 9.0$ Hz), 111.50 (dd, $J_{F-C} = 22.8, 3.9$ Hz), 82.07, 64.80, 42.68, 33.65, 24.27. ESI-MS calcd for $C_{20}H_{20}F_2N_2O_3$ $[M+H]^+$, 375.2, $[M+NH_4]^+$, 392.2, found 375.4, 392.3.

5.3.12. 2,6-Difluoro-3-((5-(4-(tert-butyl)phenyl)-4,5-dihydroisoxazol-3-yl)methoxy)benzamide (B12)

Waxy solid; 1H NMR (600 MHz, DMSO-*d*₆) δ 8.14 (s, 1H), 7.87 (s, 1H), 7.39 (d, $J = 8.4$ Hz, 2H), 7.33 (td, $J = 9.3, 5.2$ Hz, 1H), 7.23 (d, $J = 8.2$ Hz, 2H), 7.11 (td, $J = 8.9, 1.8$ Hz, 1H), 5.60 (dd, $J = 11.0, 8.3$ Hz, 1H), 5.01 (s, 2H), 3.54 (dd, $J = 17.5, 11.2$ Hz, 1H), 3.04 (dd, $J = 17.5, 8.4$ Hz, 1H), 1.27 (s, 9H). ^{13}C NMR (150 MHz, DMSO-*d*₆) δ 161.63, 155.47, 152.84 (dd, $J_{F-C} = 242.1, 6.7$ Hz), 151.08, 148.64 (dd, $J_{F-C} = 248.7, 8.6$ Hz), 142.61 (dd, $J_{F-C} = 11.0, 3.3$ Hz), 138.26, 126.32, 125.83, 117.21 (d, $J_{F-C} = 4.5$ Hz), 116.99 (d, $J_{F-C} = 9.5$ Hz), 111.51 (dd, $J_{F-C} = 22.8, 3.9$ Hz), 81.92, 64.77, 42.65, 34.76, 31.56. ESI-MS calcd for $C_{21}H_{23}F_2N_2O_3$ $[M+H]^+$, 389.4, found 389.3.

5.3.13. 2,6-Difluoro-3-((5-(4-butylphenyl)-4,5-dihydroisoxazol-3-yl)methoxy)benzamide (B13)

White solid, Mp: 101–102 °C; 1H NMR (600 MHz, Chloroform-*d*) δ 7.21–7.16 (m, 4H), 7.13 (td, $J = 9.1, 5.1$ Hz, 1H), 6.90 (td, $J = 9.1, 2.0$ Hz, 1H), 5.93 (d, $J = 30.7$ Hz, 2H), 5.63 (dd, $J = 11.0, 8.5$ Hz, 1H), 4.97–4.89 (m, 2H), 3.51 (dd, $J = 17.4, 11.1$ Hz, 1H), 3.09 (dd, $J = 17.4, 8.4$ Hz, 1H), 2.60 (t, 2H), 1.61–1.58 (m, 2H), 1.39–1.31 (m, 2H), 0.92 (t, $J = 7.4$ Hz, 3H). HRMS (ESI) calcd for $C_{21}H_{23}F_2N_2O_3$ $[M+H]^+$, 389.1671, found 389.1673.

5.3.14. 2,6-Difluoro-3-((5-(3-methoxyphenyl)-4,5-dihydroisoxazol-3-yl)methoxy)benzamide (B14)

White solid, Mp: 116–120 °C; 1H NMR (600 MHz, Chloroform-*d*) δ 7.28–7.26 (m, 2H), 7.13–7.09 (td, $J = 9.1, 5.1$ Hz, 1H), 6.90–6.84 (m, 3H), 6.80–6.79 (t, $J = 2.1$ Hz, 1H), 6.00–5.96 (d, $J = 27.5$ Hz, 2H), 5.65–5.62 (dd, $J = 11.1, 8.0$ Hz, 1H), 4.93 (s, 2H), 3.80 (s, 3H), 3.56–3.51 (dd, $J = 17.4, 11.1$ Hz, 1H), 3.10–3.06 (dd, $J = 17.4, 8.0$ Hz,

1H). ^{13}C NMR (150 MHz, DMSO-*d*₆) δ 161.68, 159.90, 155.52, 152.87 (dd, $J_{F-C} = 242.1, 6.6$ Hz), 148.65 (dd, $J_{F-C} = 248.8, 8.4$ Hz), 142.97, 142.64 (dd, $J_{F-C} = 11.0, 3.2$ Hz), 130.27, 118.51, 117.19 (dd, $J_{F-C} = 25.0, 20.4$ Hz), 116.91 (dd, $J_{F-C} = 9.3, 2.2$ Hz), 114.02, 111.98, 111.49 (dd, $J_{F-C} = 23.1, 3.8$ Hz), 81.91, 64.73, 55.50, 42.94. ESI-MS calcd for $C_{18}H_{16}F_2N_2O_4$ $[M+H]^+$, 363.1, $[M+NH_4]^+$, 380.1, found 363.3, 380.4.

5.3.15. 2,6-Difluoro-3-((5-(2-ethoxyphenyl)-4,5-dihydroisoxazol-3-yl)methoxy)benzamide (B15)

White solid, Mp: 124–128 °C; 1H NMR (600 MHz, Chloroform-*d*) δ 7.31–7.29 (dd, $J = 7.5, 1.7$ Hz, 1H), 7.26–7.24 (dd, $J = 7.8, 1.8$ Hz, 1H), 7.13–7.09 (td, $J = 9.1, 5.1$ Hz, 1H), 6.93–6.85 (m, 3H), 5.94–5.86 (m, 3H), 4.93–4.86 (m, 2H), 4.10–4.02 (m, 2H), 3.57–3.52 (dd, $J = 17.5, 11.3$ Hz, 1H), 3.01–2.97 (dd, $J = 17.5, 7.8$ Hz, 1H), 1.42–1.36 (t, $J = 7.0$ Hz, 3H). ^{13}C NMR (150 MHz, DMSO-*d*₆) δ 161.60, 155.92, 155.39, 152.76 (dd, $J_{F-C} = 242.1, 6.7$ Hz), 148.54 (dd, $J_{F-C} = 248.8, 8.4$ Hz), 142.64 (dd, $J_{F-C} = 11.0, 3.2$ Hz), 129.70, 129.01, 126.78, 120.63, 117.14 (dd, $J_{F-C} = 25.1, 20.4$ Hz), 116.81 (d, $J_{F-C} = 9.3$ Hz), 112.46, 111.45 (dd, $J_{F-C} = 23.1, 3.9$ Hz), 78.17, 64.74, 63.84, 42.03, 15.00. ESI-MS calcd for $C_{19}H_{18}F_2N_2O_4$ $[M+H]^+$, 377.1, $[M+NH_4]^+$, 394.1, found 377.3, 394.2.

5.3.16. 2,6-Difluoro-3-((5-(3-ethoxyphenyl)-4,5-dihydroisoxazol-3-yl)methoxy)benzamide (B16)

Waxy solid, Mp: 106–110 °C; 1H NMR (600 MHz, Chloroform-*d*) δ 7.26–7.24 (d, $J = 7.9$ Hz, 1H), 7.13–7.10 (td, $J = 9.1, 5.1$ Hz, 1H), 6.90–6.78 (m, 4H), 6.01–5.95 (d, $J = 35.2$ Hz, 2H), 5.64–5.61 (dd, $J = 11.1, 8.0$ Hz, 1H), 4.92 (s, 2H), 4.05–3.98 (qd, $J = 7.0, 3.7$ Hz, 2H), 3.55–3.51 (dd, $J = 17.4, 11.2$ Hz, 1H), 3.10–3.05 (dd, $J = 17.4, 8.0$ Hz, 1H), 1.42–1.39 (t, $J = 7.0$ Hz, 3H). ^{13}C NMR (151 MHz, DMSO-*d*₆) δ 161.68, 159.18, 155.49, 152.86 (dd, $J_{F-C} = 242.3, 6.7$ Hz), 148.65 (dd, $J_{F-C} = 248.8, 8.4$ Hz), 142.96, 142.64 (dd, $J_{F-C} = 11.0, 3.3$ Hz), 130.24, 118.43, 117.20 (dd, $J_{F-C} = 24.9, 20.4$ Hz), 116.87 (d, $J_{F-C} = 9.2$ Hz), 114.45, 112.46, 111.49 (dd, $J_{F-C} = 23.1, 3.8$ Hz), 81.92, 64.71, 63.45, 42.93, 15.06. ESI-MS calcd for $C_{19}H_{18}F_2N_2O_4$ $[M+H]^+$, 377.1, $[M+NH_4]^+$, 394.1, found 377.4, 394.3.

5.3.17. 2,6-Difluoro-3-((5-(4-ethoxyphenyl)-4,5-dihydroisoxazol-3-yl)methoxy)benzamide (B17)

White solid, Mp: 106–109 °C; 1H NMR (600 MHz, Chloroform-*d*) δ 7.19–7.18 (m, 2H), 7.15–7.11 (td, $J = 9.1, 5.1$ Hz, 1H), 6.91–6.84 (m, 3H), 5.97–5.93 (d, $J = 23.2$ Hz, 2H), 5.62–5.59 (dd, $J = 10.9, 8.6$ Hz, 1H), 4.93 (s, 2H), 4.05–4.01 (q, $J = 7.0$ Hz, 2H), 3.51–3.46 (dd, $J = 17.4, 11.0$ Hz, 1H), 3.09–3.05 (dd, $J = 17.4, 8.5$ Hz, 1H), 1.42–1.40 (t, $J = 7.0$ Hz, 3H). ^{13}C NMR (150 MHz, DMSO-*d*₆) δ 161.66, 158.91, 155.48, 152.86 (dd, $J_{F-C} = 242.1, 6.7$ Hz), 148.67 (dd, $J_{F-C} = 248.8, 8.4$ Hz), 142.62 (dd, $J_{F-C} = 10.8, 3.2$ Hz), 132.88, 128.08, 117.20 (d, $J_{F-C} = 4.5$ Hz), 117.02 (d, $J_{F-C} = 8.3$ Hz), 114.89, 111.52 (dd, $J_{F-C} = 23.2, 3.9$ Hz), 81.99, 64.83, 63.51, 42.49, 15.07. ESI-MS calcd for $C_{19}H_{18}F_2N_2O_4$ $[M+H]^+$, 377.1, $[M+NH_4]^+$, 394.1, found 377.4, 394.3.

5.3.18. 2,6-Difluoro-3-((5-(4-propoxyphenyl)-4,5-dihydroisoxazol-3-yl)methoxy)benzamide (B18)

White solid, Mp: 76–78 °C; 1H NMR (600 MHz, Chloroform-*d*) δ 7.19–7.18 (m, 2H), 7.15–7.11 (td, $J = 9.1, 5.1$ Hz, 1H), 6.91–6.86 (m, 3H), 5.97–5.96 (d, $J = 9.8$ Hz, 2H), 5.62–5.59 (dd, $J = 10.9, 8.6$ Hz, 1H), 4.93 (s, 2H), 3.92–3.90 (t, $J = 6.6$ Hz, 2H), 3.51–3.46 (dd, $J = 17.4, 11.0$ Hz, 1H), 3.09–3.05 (dd, $J = 17.4, 8.5$ Hz, 1H), 1.83–1.77 (h, $J = 7.3$ Hz, 2H), 1.04–1.02 (t, $J = 7.4$ Hz, 3H). ESI-MS calcd for $C_{20}H_{20}F_2N_2O_4$ $[M+H]^+$, 391.1, $[M+NH_4]^+$, 408.1, found 391.3, 408.4.

5.4. *In vitro* antibacterial assay

The MIC values of the synthesized compounds was determined in a 96-well microplate using the broth microdilution method recommended in the Clinical and Laboratory Standards Institute (CLSI) guidelines.¹⁸ The measurements were performed as previously described.¹⁶

5.5. Minimum bactericidal concentration (MBC) assay

The measurements were performed as previously described.¹⁶

5.6. Time-kill curve assay

The measurements were performed as previously described at various concentrations of **A16** or comparator drug.¹⁶

5.7. Visualization of bacterial morphology

B. subtilis ATCC9372 and *S. aureus* ATCC CI were selected as tested bacterial strains, and the measurements were performed as previously described.¹⁶

5.8. FtsZ polymerization assay

B. subtilis FtsZ was cloned, overexpressed and purified as previously described.¹⁹ The polymerization of BsFtsZ protein was monitored using a microtiter plate-based light-scattering assay in which changes in light scattering are reflected by corresponding changes in absorbance at 340 nm (A_{340})²⁶. The experimental method was referred to our previous study.¹⁶

5.9. Compound's stability study in vitro mouse plasma

The fresh mice plasma was prepared by drawing blood, anticoagulation, and centrifugation. The experimental solution of the tested compound at concentrations of 25 µg/mL was prepared from 2.56 mg/mL DMSO stock solutions in freshly prepared mouse plasma and then incubated at 37 °C. 20 µL of the solution was added to 60 µL of methanol at a specific time point throughout 24 h. The obtained samples were centrifuged at 12000 rpm for 4 min, and then the supernatants of each sample were assessed using LC-MS.

For the LC-MS measurement, a reverse-phase Diamonsil C18 column was used on a Thermo Ultimate 3000 series LC-MS equipped with a DAD detector (set at 254 nm). The column size was 150 × 4.6 mm, with the particle and pore sizes being 5 µm and 100 Å, respectively. The column temperature was controlled under 35 °C. A 20 µL sample of each experimental solution was injected, and a flow rate of 0.3 mL/min was applied, along with an isocratic condition of 10–90% acetonitrile and water in the mobile phase. Peak areas were determined using the Xcalibur.

5.10. *In vivo* efficacy models of infection

Antistaphylococcal efficacy *in vivo* was assessed in a mouse blood model of infection with a clinical isolated *S. aureus* (MDRS). All experimental procedures conformed to the animal experiment guidelines of the Animal Care and Welfare Committee of Shandong University. Three groups of four KM mice with an average weight of 20 g were infected intravenously with an inoculum of bacterial (0.15 mL of saline containing 8.5×10^8 CFU). Compounds (or the vehicle control) were administered i.v. at the doses of 10 mg/kg and three times a day. The vehicle contained 2% DMAC, 30% PEG400/PG (v/v, 1:1), and 5% HPβCD in water (final). After 48 h, the mouse were anaesthetized, blood was collected from retro-orbital plexus and then 0.1 mL were spread on to TSA plates for CFU enumeration. The numbers of CFU

were determined from each plate following overnight incubation.

5.11. MTT cytotoxicity assay

The cytotoxicity of compounds was assessed in human cervical cancer (Hela) cells using a 48 h continuous 3-(4,5-dimethylthiazol-2-yl)-2,5-diphenyltetrazolium bromide (MTT) assay as previously described²⁷. The experimental method was referred to our previous study.¹⁶

5.12. Computational analysis

The molecular docking study was performed using Le-Dock. Molecular ligand **A16**, **B13** and **A26_{pre}** were constructed and saved as Mol2 files by Chembio3D software. The FtsZ crystal structure (PDB code: 3vob) was obtained from Protein Data Bank (PDB) and then prepared for docking by using Le-Dock. The docking results were visually inspected and analyzed using Pymol (version 1.5).

Declaration of Competing Interest

The authors declare that they have no known competing financial interests or personal relationships that could have appeared to influence the work reported in this paper.

Acknowledgements

This research was supported financially by the National Natural Science Foundation of China (81973179 and 81673284), Key Research and Development Project of Shandong Province (2017CXGC1401) and the China-Australia Centre for Health Sciences Research (CACHSR no. 2019GJ05).

Appendix A. Supplementary material

Supplementary data to this article can be found online at <https://doi.org/10.1016/j.bmc.2020.115729>.

References

- Hughes D, Karlen A. Discovery and preclinical development of new antibiotics. *Ups J Med Sci.* 2014;119:162–169.
- Odagiri T, Inagaki H, Nagamochi M, Kitamura T, Komoriya S, Takahashi H. Design, synthesis, and biological evaluation of novel 7-[(3 aS,7 aS)-3 a-Aminohexahydroprano[3,4- c]pyrrol-2(3 H)-yl]-8-methoxyquinolines with Potent Antibacterial Activity against Respiratory Pathogens. *J Med Chem.* 2018;61:7234–7244.
- Dhanda G, Sarkar P, Samaddar S, Haldar J. Battle against vancomycin-resistant bacteria: recent developments in chemical strategies. *J Med Chem.* 2019;62:3184–3205.
- Panda D, Bhattacharya D, Gao QH, et al. Identification of agents targeting FtsZ assembly. *Future Med Chem.* 2016;8:1111–1132.
- Schaffner-Barbero C, Martin-Fontecha M, Chacon P, Andreu JM. Targeting the assembly of bacterial cell division protein FtsZ with small molecules. *ACS Chem Biol.* 2012;7:269–277.
- Hurley KA, Santos TM, Nepomuceno GM, Huynh V, Shaw JT, Weibel DB. Targeting the bacterial division protein FtsZ. *J Med Chem.* 2016;59:6975–6998.
- Groundwater PW, Narlawar R, Liao VW, et al. A carbocyclic curcumin inhibits proliferation of gram-positive bacteria by targeting FtsZ. *Biochemistry.* 2017;56:514–524.
- Fang Z, Zheng S, Chan KF, et al. Design, synthesis and antibacterial evaluation of 2,4-disubstituted-6-thiophenyl-pyrimidines. *Eur J Med Chem.* 2019;161:141–153.
- Stokes NR, Baker N, Bennett JM, et al. An improved small-molecule inhibitor of FtsZ with superior *in vitro* potency, drug-like properties, and *in vivo* efficacy. *Antimicrob Agents Chemother.* 2013;57:317–325.
- Haydon DJ, Bennett JM, Brown D, et al. Creating an antibacterial with *in vivo* efficacy: synthesis and characterization of potent inhibitors of the bacterial cell division protein FtsZ with improved pharmaceutical properties. *J Med Chem.* 2010;53:3927–3936.
- Ohashi Y, Chijiwa Y, Suzuki K, et al. The lethal effect of a benzamide derivative, 3-methoxybenzamide, can be suppressed by mutations within a cell division gene, *ftsZ*, in *Bacillus subtilis*. *J Bacteriol.* 1999;181:1348–1351.
- Kaul M, Mark L, Zhang Y, Parhi AK, Lavoie EJ, Pilch DS. An FtsZ-targeting prodrug with oral antistaphylococcal efficacy *in vivo*. *Antimicrob Agents Chemother.*

- 2013;57:5860–5869.
13. Kaul M, Mark L, Zhang Y, Parhi AK, LaVoie EJ, Pilch DS. Pharmacokinetics and in vivo antistaphylococcal efficacy of TXY541, a 1-methylpiperidine-4-carboxamide prodrug of PC190723. *Biochem Pharmacol*. 2013;86:1699–1707.
 14. Kaul M, Zhang Y, Parhi AK, et al. Enterococcal and streptococcal resistance to PC190723 and related compounds: molecular insights from a FtsZ mutational analysis. *Biochimie*. 2013;95:1880–1887.
 15. Kaul M, Mark L, Zhang Y, et al. TXA709, an FtsZ-targeting benzamide prodrug with improved pharmacokinetics and enhanced in vivo efficacy against methicillin-resistant *Staphylococcus aureus*. *Antimicrob Agents Chemother*. 2015;59:4845–4855.
 16. Bi F, Song D, Zhang N, et al. Design, synthesis and structure-based optimization of novel isoxazole-containing benzamide derivatives as FtsZ modulators. *Eur J Med Chem*. 2018;159:90–103.
 17. Machetti F, Cecchi L, Trogu E, De Sarlo F. Isoxazoles and Isoxazolines by 1, 3-dipolar cycloaddition: base-catalysed condensation of primary nitro compounds with dipolarophiles. *Eur J Org Chem*. 2007;2007:4352–4359.
 18. Wikler MA, Hindler JF, Cookerill FR, Patel JB, Bush K, Powell M. Methods for dilution antimicrobial susceptibility tests for bacteria that grow aerobically. *Clin Lab Standards Institute*. 2009::M07–M8.
 19. Haydon DJ, Stokes NR, Ure R, et al. An inhibitor of FtsZ with potent and selective anti-staphylococcal activity. *Science*. 2008;321:1673–1675.
 20. Bi F, Guo L, Wang Y, et al. Design, synthesis and biological activity evaluation of novel 2,6-difluorobenzamide derivatives through FtsZ inhibition. *Bioorg Med Chem Lett*. 2017;27:958–962.
 21. Andreu JM, Schaffner-Barbero C, Huecas S, et al. The antibacterial cell division inhibitor PC190723 is an FtsZ polymer-stabilizing agent that induces filament assembly and condensation. *J Biol Chem*. 2010;285:14239–14246.
 22. Adams DW, Wu LJ, Czaplowski LG, Errington J. Multiple effects of benzamide antibiotics on FtsZ function. *Mol Microbiol*. 2011;80:68–84.
 23. Hegde SS, Difuntorum S, Skinner R, Trumbull J, Krause KM. Efficacy of telavancin against glycopeptide-intermediate *Staphylococcus aureus* in the neutropenic mouse bacteraemia model. *J Antimicrob Chemother*. 2009;63:763–766.
 24. Fujita J, Maeda Y, Mizohata E, et al. Structural flexibility of an inhibitor overcomes drug resistance mutations in *Staphylococcus aureus* FtsZ. *ACS Chem Biol*. 2017;12:1947–1955.
 25. Wang YN, Bheemanaboina RRY, Gao WW, Kang J, Cai GX, Zhou CH. Discovery of benzimidazole-quinolone hybrids as new cleaving agents toward drug-resistant *Pseudomonas aeruginosa* DNA. *ChemMedChem*. 2018;13:1004–1017.
 26. Kaul M, Parhi AK, Zhang Y, et al. A bactericidal guanidinomethyl biaryl that alters the dynamics of bacterial FtsZ polymerization. *J Med Chem*. 2012;55:10160–10176.
 27. Ekins S, Reynolds RC, Kim H, et al. Bayesian models leveraging bioactivity and cytotoxicity information for drug discovery. *Chem Biol*. 2013;20:370–378.